Resolving steady-state multiplicities for diffusion with surface chemical reaction by invoking the Prigogine principle of minimum entropy production

CrossMark

Rajamani Krishna

Van't Hoff Institute for Molecular Sciences, University of Amsterdam, Science Park 904, 1098 XH Amsterdam, The Netherlands

A B S T R A C T

The process of coupled multicomponent diffusion and surface reaction is described by combining the Maxwell–Stefan (M–S) and Langmuir–Hinshelwood (L–H) formulations. Five different systems are investigated: epoxidation of ethene $C_2H_4 + \frac{1}{2}O_2 \rightleftarrows C_2H_4O$, oxidation of carbon monoxide $CO + \frac{1}{2}O_2 \rightleftarrows CO_2$, hydrogenation of ethene $H_2 + C_2H_4 \rightleftarrows C_2H_6$, CO methanation $CO + 3H_2 \rightleftarrows CH_4 + H_2O$, and chemical vapor deposition $WF_6 + 2SiH_4 \rightarrow W_{(s)} + 2SiHF_3 + 3H_2$. For isothermal, isobaric operations under steady-state conditions, multiplicity of solutions are found for all five reaction systems. The origin of the multiplicities is traceable to the non-linear characteristics of the L–H kinetics. Application of the Prigogine principle of minimum entropy production indicates that the low-conversion steady-state is the stable one that can be realized in practice. The reported results have important consequences for modelling and design of chemical vapor deposition processes and micro-channel reaction devices consisting of thin catalyst coatings on the walls.

© 2017 Institution of Chemical Engineers. Published by Elsevier B.V. All rights reserved.

1. Introduction

There is increasing interest and research activity in the application of micro-channel reaction devices in a variety of processes such as epoxidation of ethene, methylchloride synthesis, partial oxidation of methane, methanol steam reforming, dehydrogenation of ethane, methanation of carbon oxides, production of phosgene, and Fischer–Tropsch synthesis (Brooks et al., 2007; Deshmukh et al., 2010; Görke et al., 2005; Hernández Carucci et al., 2010; Kiwi-Minsker and Renken, 2005; Pennline et al., 1981; Russo et al., 2015; Schmidt et al., 2013; Venkataraman et al., 2002). A common characteristic of such micro-reactors, that have thin catalyst coatings on the walls, is that the transport of reactants and products towards and away from the catalyst surface is subject to diffusional limitations (Gervais and Jensen, 2006; Russo et al., 2015; Schmidt et al., 2013). In chemical vapor deposition (CVD) processes, the rates of deposition on metal substrates (wafers)

are dictated by molecular diffusion in the gas phase adjacent to the substrate (Kuijlaars et al., 1995).

If the surface reaction follows the generic scheme,

$$\nu_1 A_1 + \nu_2 A_2 + \nu_3 A_3 + \ldots \nu_n A_n = 0 \tag{1}$$

the steady-state transfer fluxes, N_i, from the bulk gas mixture to the catalyst surface are coupled to one another because the ratios of the fluxes are constrained by the reaction stoichiometry:

$$\frac{N_1}{\nu_1} = \frac{N_2}{\nu_2} = \frac{N_3}{\nu_3} = \ldots = \frac{N_n}{\nu_n} \tag{2}$$

The surface reaction influences the transfer fluxes N_i by altering the partial pressures adjacent to the surface $p_{i\delta}$ in the gas phase. The surface concentrations are different from the corresponding bulk phase concentrations because of diffusional limitations and differences in

the adsorption strengths of the constituent species. Simply put, the transfer fluxes influence surface reaction rates and the kinetics, in turn, influences the transfer fluxes. One of the imprtant consequences of such coupling effects has been highlighted by Löwe and Bub (1976); they present a theoretical analysis of gaseous diffusion with surface reaction $A_1 + 2A_2 \rightleftarrows A_3$, that is described by the Langmuir–Hinshelwood (L–H) kinetic prescription,

$$Rate = \frac{k p_{1\delta} p_{2\delta}}{\left(1 + K_1 p_{1\delta} + K_2 p_{2\delta}\right)^2} \tag{3}$$

For diffusion in the bulk gas phase, Löwe and Bub (1976) employed a simplified Maxwell–Stefan (M–S) description,

$$-\frac{dy_i}{dz} = \sum_{\substack{j=1 \\ j \neq i}}^{n} \frac{y_j N_i - y_i N_j}{c_t Ð}; \quad i = 1, 2, \ldots n \tag{4}$$

assuming the diffusivities of the three constituent pairs to be equal to one another, $Ð_{12} = Ð_{13} = Ð_{23} = Ð$. For isothermal, isobaric operations at steady-state conditions, Löwe and Bub (1976) demonstrated the possibility of multiple steady-states for chosen set of diffusion and reaction parameters. For elucidating the observed multiplicities, Fig. 1a presents calculations of the surface reaction rate, using the L–H expression (3); the mole fractions of A_2 at the catalyst surface $y_{2\delta}$ are varied from 0 to 0.4, maintaining the mole fraction of A_1 at the catalyst surface at $y_{1\delta} = 0.62$; the strong non-linear dependence of the reaction rate on $y_{2\delta}$ is evident. For the chosen bulk gas phase mole fractions $y_{10} = 0.6$, $y_{20} = 0.4$, $y_{30} = 0$, the flux of A_3 directed away the catalyst surface will decrease with increasing value of $y_{2\delta}$. There are three intersection points for the surface reaction rate with the transfer flux, indicating the feasibility of three different steady-state solutions; the composition profiles in the gas "film", corresponding to the three states are shown in Fig. 1b. The work reported by Löwe and Bub (1976) is distinctly different from other publications on multiplicity in reacting systems (Oh et al., 1979; Uppal and Ray, 1977; Wedel and Luss, 1984; Witmer et al., 1986) in that isothermal, isobaric conditions prevail, and the diffusion resistance is *external* to the catalyst surface. Their analysis is potentially relevant to the micro-channel reactors in which diffusion to the catalyst layer is invariably of importance (Gervais and Jensen, 2006; Russo et al., 2015; Schmidt et al., 2013).

The assumption that the binary pair diffusivities are equal to one another is overly restrictive and not justifiable in many reaction systems of practical interest. For example, in the CVD process for W deposition on Si substrate, $WF_6 + 2SiH_4 \rightarrow W_{(s)} + 2SiHF_3 + 3H_2$, the gas phase mixture consists of four species WF_6 (1), SiH_4 (2), $SiHF_3$ (3), and H_2 (4), whose molar masses are, respectively, 297.8, 32.1, 104.1, and $2\,g\,mol^{-1}$. Using the Fuller–Schettler–Giddings estimation procedure (Fuller et al., 1966; Rajagopal and Rao, 2004), the M–S diffusivities of the constituent binary pairs at typical operating conditions of temperature $T = 673\,K$ and the total pressure $p_t = 100\,Pa$ are $Ð_{12} = 0.026$; $Ð_{13} = 0.013$; $Ð_{14} = 0.152$; $Ð_{23} = 0.031$; $Ð_{24} = 0.24$; $Ð_{34} = 0.172\,m^2\,s^{-1}$; the pair diffusivities $Ð_{ij}$ differ by more than one order of magnitude. Large differences in the binary pair diffusivities enhances the "coupling" between constituent fluxes (Krishna, 2015, 2017; Krishna and van Baten, 2016).

The first objective of our investigation is to extend the Löwe/Bub analysis by using a more rigorous model for transfer fluxes using the Maxwell–Stefan formulation, taking due account of differences in pair diffusivities (Kleijn and Hoogendoorn, 1991; Krishna, 1977, 2015, 2017; Krishna and van Baten, 2016; Kuijlaars et al., 1995; Wesselingh and Krishna, 2000),

$$-\frac{dy_i}{dz} = \sum_{\substack{j=1 \\ j \neq i}}^{n} \frac{y_j N_i - y_i N_j}{c_t Ð_{ij}}; \quad i = 1, 2, \ldots n \tag{5}$$

The M–S diffusivities of the constituent binary pairs are subject to the symmetry constraint imposed by the Onsager Reciprocal Relations:
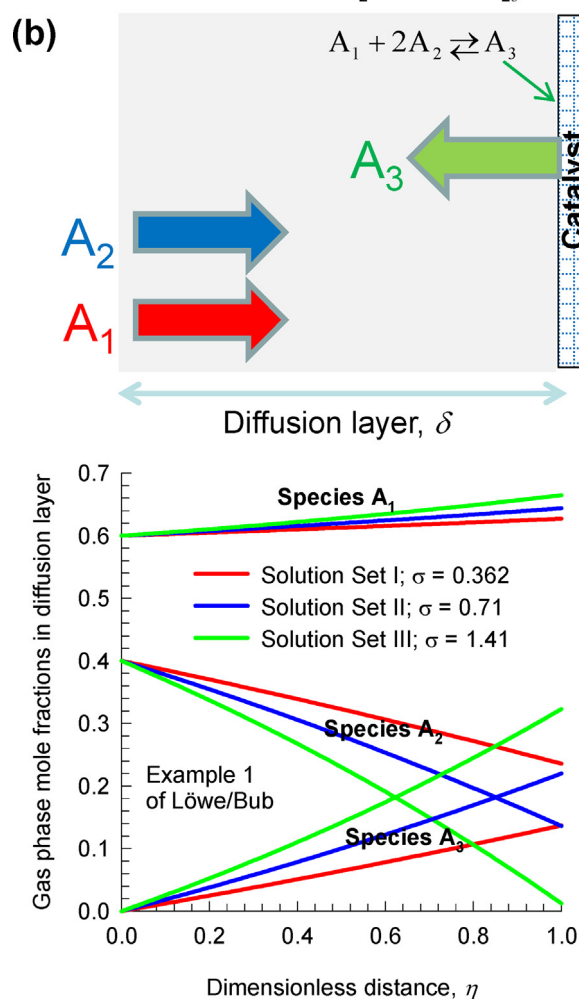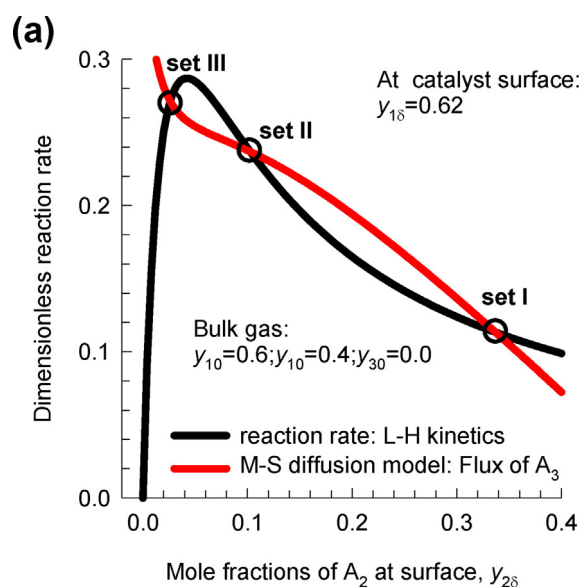

Fig. 1 – Calculations of the dimensionless surface reaction rate, following the L–H kinetic expression used by Löwe and Bub (1976) in their Example 1. The calculations are presented for mole fraction of A_1 at the catalyst surface fixed at the value $y_{1\delta} = 0.62$. The mole fractions of A_2 at the catalyst surface are varied from 0 to 0.4. Also plotted is the flux of A_3 directed away from the catalyst; the flux calculations use Eq. (17). (b) Composition profiles in the gas film external to the catalyst surface, corresponding to the Solution sets I, II, and III; these calculations are based in Eq. (16). The dimensionless rates of entropy production σ for the three sets are also indicated. Further calculation details are provided in Supplementary material.

$Đ_{ij} = Đ_{ji}$. Exact analytic solutions are derived for the combined set of M–S/L–H equations; these are used to analyze five different reaction systems of industrial importance: epoxidation of ethene $C_2H_4 + \frac{1}{2}O_2 \rightleftarrows C_2H_4O$, oxidation of carbon monoxide $CO + \frac{1}{2}O_2 \rightleftarrows CO_2$, hydrogenation of ethene $H_2 + C_2H_4 \rightleftarrows C_2H_6$, CO methanation $CO + 3H_2 \rightleftarrows CH_4 + H_2O$, and chemical vapor deposition $WF_6 + 2SiH_4 \rightarrow W_{(s)} + 2SiHF_3 + 3H_2$. We aim to demonstrate the possibility of steady-state multiplicities in each reaction system.

The second objective is to resolve the issue of multiplicities by invoking the Prigogine principle of minimum entropy production (Krishna, 2017; Prigogine, 1961). This principle affords a simple and "cheap" approach to determine the physically realizable solution because its use obviates the need for undertaking a detailed stability analysis such as that reported by Löwe and Bub (1976).

Supplementary material accompanying the manuscript provides (a) detailed derivation of the analytic solution to M–S equations describing diffusion with surface reaction, and (b) numerical techniques and input data used to demonstrate multiplicity of steady-states in the five different reaction systems.

2. Definition and calculation of effective diffusivities

For the analysis of gas phase diffusion with surface reaction, it is convenient to define "effective" diffusivities, $D_{i,eff}$ for each component i in the n-component mixture,

$$N_i = -c_t D_{i,eff} \frac{dy_i}{dz}; \quad i = 1, 2, \ldots n \tag{6}$$

Eqs. (2) and (5) allow us to obtain an explicit expression for the effective diffusivities,

$$\frac{1}{D_{i,eff}} == \sum_{\substack{j=1 \\ j \neq i}}^{n} \frac{x_j}{Đ_{ij}} \left(1 - \frac{y_i N_j}{y_j N_i}\right); \quad i = 1, 2, \ldots n \tag{7}$$

The effective diffusivities are dependent on both compositions, and the flux ratios. To emphasize this point, Fig. 2 presents calculations of $D_{i,eff}$ in four different reaction systems. The effective diffusivity of H_2 participating in $WF_6 + 2SiH_4 \rightarrow W_{(s)} + 2SiHF_3 + 3H_2$ reaction is about an order of magnitude higher than that of WF_6. For methanation of carbon monoxide, $CO + 3H_2 \rightleftarrows CH_4 + H_2O$, the effective diffusivity of H_2 is about a factor 3 higher than that of CO; the product CH_4 has the lowest effective diffusivity because its motion is in a direction opposite to the total mixture flux, $N_t = N_1 + 3N_1 + N_1 - N_1 = 2N_1$. For hydrogenation of ethene $H_2 + C_2H_4 \rightleftarrows C_2H_6$, the effective diffusivity of H_2 is about a factor 5 higher than that of C_2H_6 whose flux opposes that of the total mixture, $N_t = N_1 + N_1 - N_1 = N_1$.

Even if the binary pair M–S diffusivities are equal to one another, $Đ_{12} = Đ_{13} = Đ_{14} = Đ_{23} = Đ_{34} \ldots = Đ$, as assumed in the Löwe/Bub analysis, it is easy to check that the effective diffusivity of all components are not equal to one another:

$$\frac{1}{D_{i,eff}} = \sum_{\substack{j=1 \\ j \neq i}}^{n} \frac{x_j}{Đ} \left(1 - \frac{y_i N_j}{y_j N_i}\right) \tag{8}$$

In this scenario, the differences in the effective diffusivity values, originate from the differing flux ratios of individual species. For ethene epoxidation $C_2H_4 + \frac{1}{2}O_2 \rightleftarrows C_2H_4O$ at $T = 573\,K$ and the total pressure $p_t = 200\,kPa$, the M–S diffusivities of the constituent binary pairs are very close to

one another: $Đ_{12} = 2.45$; $Đ_{13} = 1.64$; $Đ_{23} = 2.08 \times 10^{-5}\,m^2\,s^{-1}$. The effective diffusivity of C_2H_4O is, however, about a factor 2 lower than that of O_2 (see Fig. 2d); this is due to the fact that the transfer of C_2H_4O is in a direction opposite to the net mixture flux $N_t = N_1 + \frac{1}{2}N_1 - N_1 = \frac{1}{2}N_1$, that is directed towards the catalyst surface. Eq. (7) also holds if there are multiple reactions occurring at the catalytic surface. In this case, the flux ratios are dependent on both the reaction stoichiometries, and the relative rates of the reactions at the surface; detailed derivations are provided in Supplementary material.

3. Exact analytic solution to the Maxwell–Stefan equations

For isothermal, isobaric steady-state diffusion across a "film" of thickness δ, we define a dimensionless distance: $\eta = \frac{z}{\delta}$. The bulk vapor compositions are specified as follows $\eta = 0$; $z = 0$; $(y) = (y_0)$. At the other end of the film, the boundary conditions are $\eta = 1$; $z = \delta$; $(y) = (y_\delta)$; at this position we have the surface reaction, as represented by Eq. (1).

The mole fractions sum to unity, and therefore only $n - 1$ of Eq. (5) are independent. We define an $n - 1 \times n - 1$ dimensional square matrix $[\Phi]$:

$$\Phi_{ii} = \left(\frac{\nu_i}{\nu_1 Đ_{in}} + \sum_{k=1; k \approx i}^{k=n} \frac{\nu_k}{\nu_1 Đ_{ik}}\right) \frac{\delta}{c_t} N_1;$$
$$\Phi_{ik; k \neq i} = -\left(\frac{\nu_i}{\nu_1 Đ_{ik}} - \frac{\nu_i}{\nu_1 Đ_{in}}\right) \frac{\delta}{c_t} N_1; \quad i = 1, 2, \ldots n - 1 \tag{9}$$

and an $n - 1$ dimensional column matrix (ϕ),

$$\phi_i = -\left(\frac{\nu_i}{\nu_1 Đ_{in}}\right) \frac{\delta}{c_t} N_1; \quad i = 1, 2, \ldots n - 1 \tag{10}$$

Eq. (5) can be cast into $n - 1$ dimensional matrix notation,

$$\frac{d(y)}{d\eta} = [\Phi](y) + (\phi) \tag{11}$$

For steady-state transfer across a film, the matrices $[\Phi]$ and (ϕ) are both η-invariant. Therefore Eq. (11) represents a system of coupled *ordinary* differential equations with *constant coefficients* $[\Phi]$ and (ϕ). Following the procedure of Krishna (2017) and Krishna and Standart (1976), the system of equations can be solved analytically to obtain the mole fraction profiles within the diffusion layer,

$$(y_\eta - y_0) = -[\exp[\Phi\eta] - [I]][\exp[\Phi] - [I]]^{-1}(y_0 - y_\delta) \tag{12}$$

In Eq. (12), $[I]$ is the identity matrix with Kronecker delta δ_{ik} as elements. The composition gradient at the position η can be obtained by differentiation of Eq. (12); we get,

$$\frac{d(y_\eta)}{d\eta} = -[\Phi][\exp[\Phi\eta]][\exp[\Phi] - [I]]^{-1}(y_0 - y_\delta) \tag{13}$$

The steady-state transfer fluxes of components $1, 2, \ldots n - 1$ can be determined by combining Eqs. (6) and (13).

$$(N) = -\frac{c_t}{\delta} \left[D_{eff,\eta}\right] \frac{d(y_\eta)}{d\eta} = \frac{c_t}{\delta} \left[D_{eff,\eta}\right] [\Phi][\exp[\Phi]\eta]$$
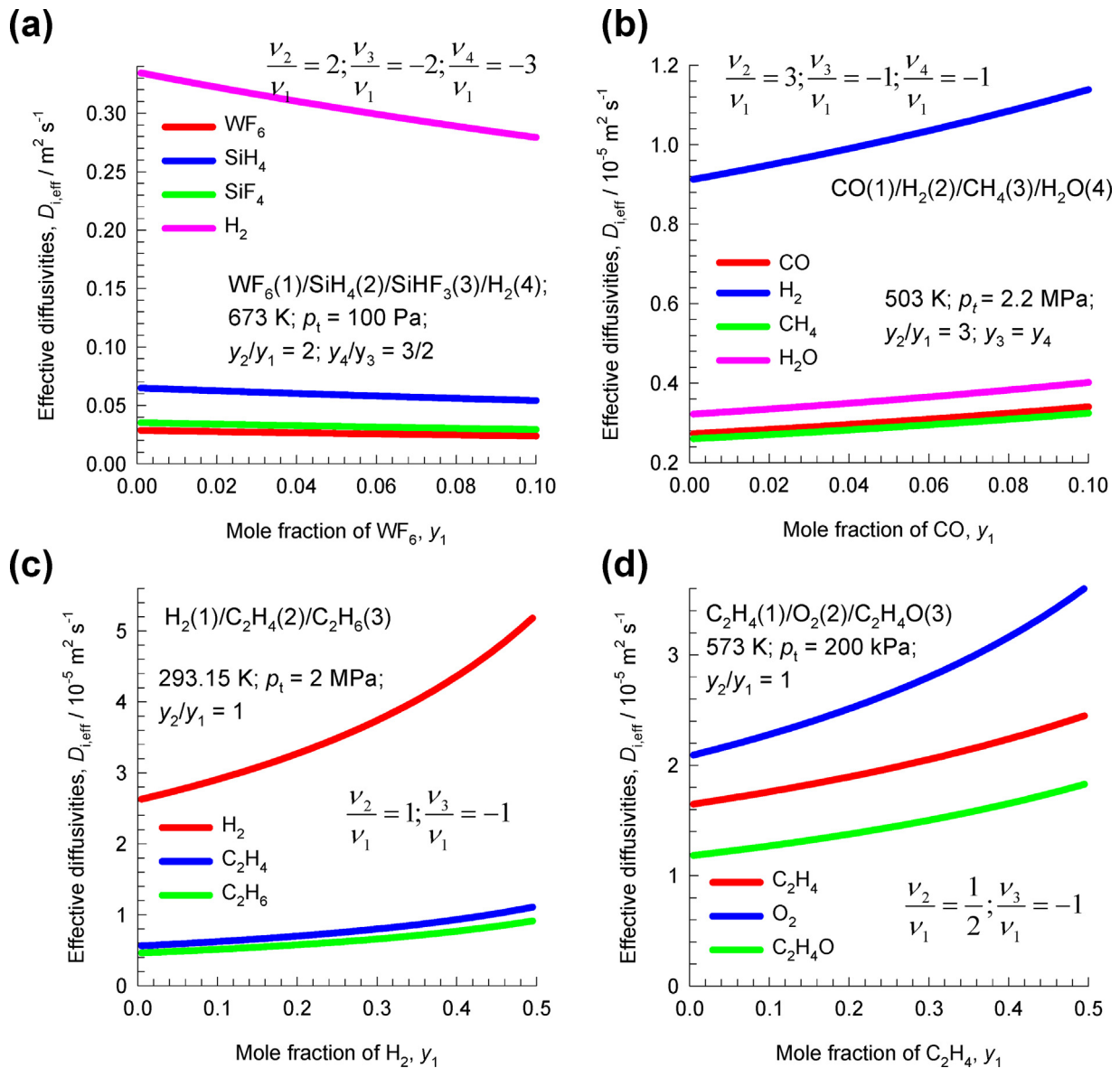$$[\exp[\Phi] - [I]]^{-1}(y_0 - y_\delta) \tag{14}$$

Fig. 2 – Calculation of the effective diffusivities of constituent species participating in (a) $WF_6 + 2SiH_4 \rightarrow W_{(s)} + 2SiHF_3 + 3H_2$ reaction at $T = 673\,K$, $p_t = 100\,Pa$, (b) $CO + 3H_2 \rightleftarrows CH_4 + H_2O$ reaction at $T = 503\,K$, $p_t = 2.2\,MPa$, (c) $H_2 + C_2H_4 \rightleftarrows C_2H_6$ reaction at $T = 293.15\,K$, $p_t = 2\,MPa$, and (d) $C_2H_4 + \frac{1}{2}O_2 \rightleftarrows C_2H_4O$ reaction at $T = 573\,K$, $p_t = 200\,kPa$. Further calculation details are provided in Supplementary material.

where the diagonal matrix of effective diffusivities matrix at position η is $\left[D_{eff,\eta}\right]$, with elements $D_{i,eff}\delta_{ik}$, is calculated from Eq. (7) using the compositions at position η. Without loss of generality, we may evaluate $\left[D_{eff,\eta}\right]$ at position $\eta = 0$, and obtain,

$$(N) = -\frac{c_t}{\delta} \left[D_{eff,\eta=0}\right] \frac{d(y)}{d\eta}\Big|_{\eta=0}$$

$$= \frac{c_t}{\delta} \left[D_{eff,\eta=0}\right] [\Phi] \left[\exp[\Phi] - [I]\right]^{-1} (y_0 - y_\delta) \qquad (15)$$

In Eq. (15), the diagonal matrix of effective diffusivities is calculated using the compositions y_{i0} at position $\eta = 0$. Though the expression (15) appears to be explicit in the fluxes, it is to be noted that the matrix factor $[\Phi] \left[\exp[\Phi] - [I]\right]^{-1}$ is also a function of the transfer fluxes. Eq. (15) may be implemented into current models for micro-channel reactors, such as that of Russo et al. (2015).

For the special scenario in which the M–S pair diffusivities are assumed to equal one another, the corresponding analytic solution to simplified set of Eq. (8) is derived by noting that $[\Phi]$ simplifies to the scalar quantity $\Phi = \left(1 + \sum\limits_{k=1;k\approx i}^{k=n} \frac{v_k}{v_1}\right) \frac{\delta N_1}{c_t Ð}$; the composition profiles in the gas film are described in this scenario by,

$$y_{i\eta} = y_{i0} - \frac{\exp(\Phi\eta) - 1}{\exp(\Phi) - 1} (y_{i0} - y_{i\delta}) \qquad (16)$$

The constituent transfer fluxes are then calculated from the set of *un-coupled* flux equations.

$$N_i = \frac{v_i}{v_1} N_1 = \frac{c_t}{\delta} D_{i,eff,\eta=0} \frac{\Phi}{\exp(\Phi) - 1} (y_{i0} - y_{i\delta}) \qquad (17)$$

In typical practical examples, the bulk vapor compositions $\eta = 0$; $z = 0$; $(y) = (y_0)$ are specified or determined from a reactor material balance. The $n - 1$ independent

compositions at the catalytic surface $\eta = 1$; $z = \delta$; $(y) = (y_\delta)$ are all unknown. Since the flux ratios are fixed, there is only one unknown flux, say N_1. At steady-state, the transfer flux equals the surface reaction rate, say expressed in terms of moles of component 1 converted per m² of surface per second,

$$N_1 = Rate(p_{1\delta}, p_{2\delta}, ...p_{n-1,\delta}) \tag{18}$$

The $n - 1$ independent compositions at the catalytic surface, $y_{i\delta}$, are obtained by simultaneous solution of Eqs. (15) and (18) using an iterative procedure with starting guesses of $y_{i\delta}$. The results reported here are obtained using the Given-Find solve block of MathCad 15 (PTC, 2013).

4. Steady-state multiplicities in five different reaction systems

Hernández Carucci et al. (2010) and Russo et al. (2015) have demonstrated the advantages of using a microreactor made of pure silver, that also acts as catalyst, for epoxidation of ethene $C_2H_4 + \frac{1}{2}O_2 \rightleftarrows C_2H_4O$ to produce ethene oxide, an important organic intermediate in the process industries. According to Russo et al. (2015), the Ag catalyzed epoxidation reaction conforms with the L–H kinetic Eq. (3). Fig. 3a presents calculations of the surface reaction rate with varying mole fraction of C_2H_4 at the catalyst surface, $y_{1\delta}$. The strong non-linear dependence of the reaction rate on the mole fraction of C_2H_4 at the catalyst surface is evident, and shows the same characteristics as that witnessed in Fig. 1a. For the chosen bulk gas phase mole fractions $y_{10} = 0.5$, $y_{20} = 0.25$, $y_{30} = 0.25$, the flux of C_2H_4 will be directed towards the catalyst surface; the flux will decrease with increasing values of $y_{1\delta}$. Also plotted in Fig. 3a are the calculations of the flux of C_2H_4 using Eq. (15). It is noteworthy that the variation of the flux of C_2H_4 with increasing $y_{1\delta}$ is not linear. The non-linearity emerges from the coupling effects inherent in the use of Eq. (15). The intersection of the two curves indicates three different solution sets. For a precise determination of the three steady-states, the set of Eqs. (15) and (18) need to be solved simultaneously. With starting estimated values correspond to the three (circled) compositions in Fig. 3a, we obtain the converged solutions:

Set I: $y_{1\delta} = 0.23246$; $y_{2\delta} = 0.14524$; $N_1 = 22.8 \, mol \, m^{-2} \, s^{-1}$,
Set II: $y_{1\delta} = 0.07452$; $y_{2\delta} = 0.0843$; $N_1 = 34.7 \, mol \, m^{-2} \, s^{-1}$, and
Set III: $y_{1\delta} = 2.85 \times 10^{-3}$; $y_{2\delta} = 0.05626$; $N_1 = 39.9 \, mol \, m^{-2} \, s^{-1}$.

Fig. 3b shows the composition profiles, determined using Eq. (12), for the three sets; the profiles become steeper for higher values of transfer fluxes, as is to be expected.

Plots of surface reaction rate and transfer flux vs surface composition of key component, analogous to Fig. 3a, are obtained for (a) Pt/Al₂O₃ catalyzed hydrogenation of ethene to produce ethane (Uppal and Ray, 1977), (b) Pt/SiO₂ catalyzed oxidation of CO to produce CO₂ (Herskowitz and Kenney, 1983), (c) Ni/Al₂O₃ catalyzed methanation of CO (Yadav and Rinker, 1993), and (d) W deposition on Si substrate (Ammerlaan et al., 1993); see Fig. 4. The detailed analyses of the steady-state multiplicities in each of these reaction systems, along with composition profiles in the gas diffusion layer, are provided in Figs. S7–S20 of Supplementary material. Even if the simplification of equal pair diffusivities is invoked and Eq. (17) is employed for flux calculations, the multiplicities persist; see Figs. S10 and S14. From an examination of the plots in Figs. 3 and 4, it is evident that the origin of the multiplicities resides in the *non-linearities* implicit in the L–H kinetics; a
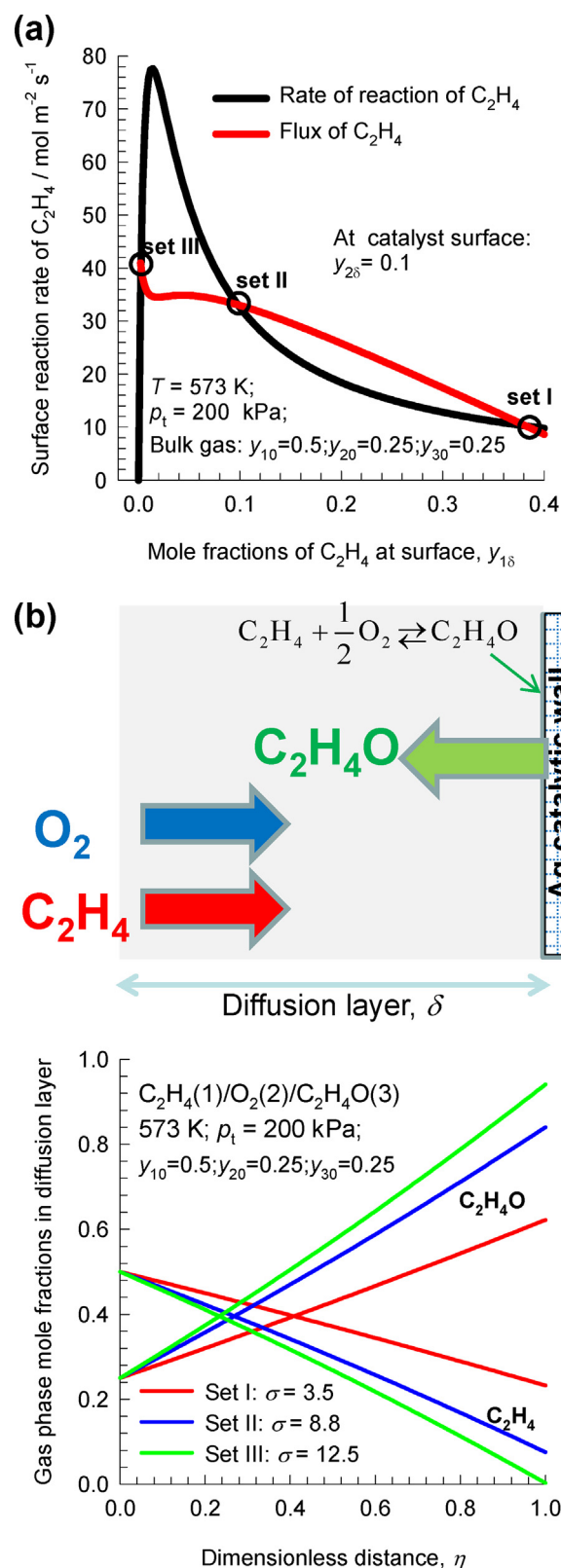

(a)

(b)

Fig. 3 – (a) Plot of the reaction rate $C_2H_4 + \frac{1}{2}O_2 \rightleftarrows C_2H_4O$ and flux of C_2H_4 versus the mole fraction of C_2H_4 at the catalyst surface, $y_{1\delta}$, applying the restraint $y_{2\delta} = 0.1$. (b) Composition profiles in the gas film external to the catalyst surface, corresponding to the Solution sets I, II, and III; the rates of entropy production σ for the three sets are also indicated. Further calculation details are provided in Supplementary material.
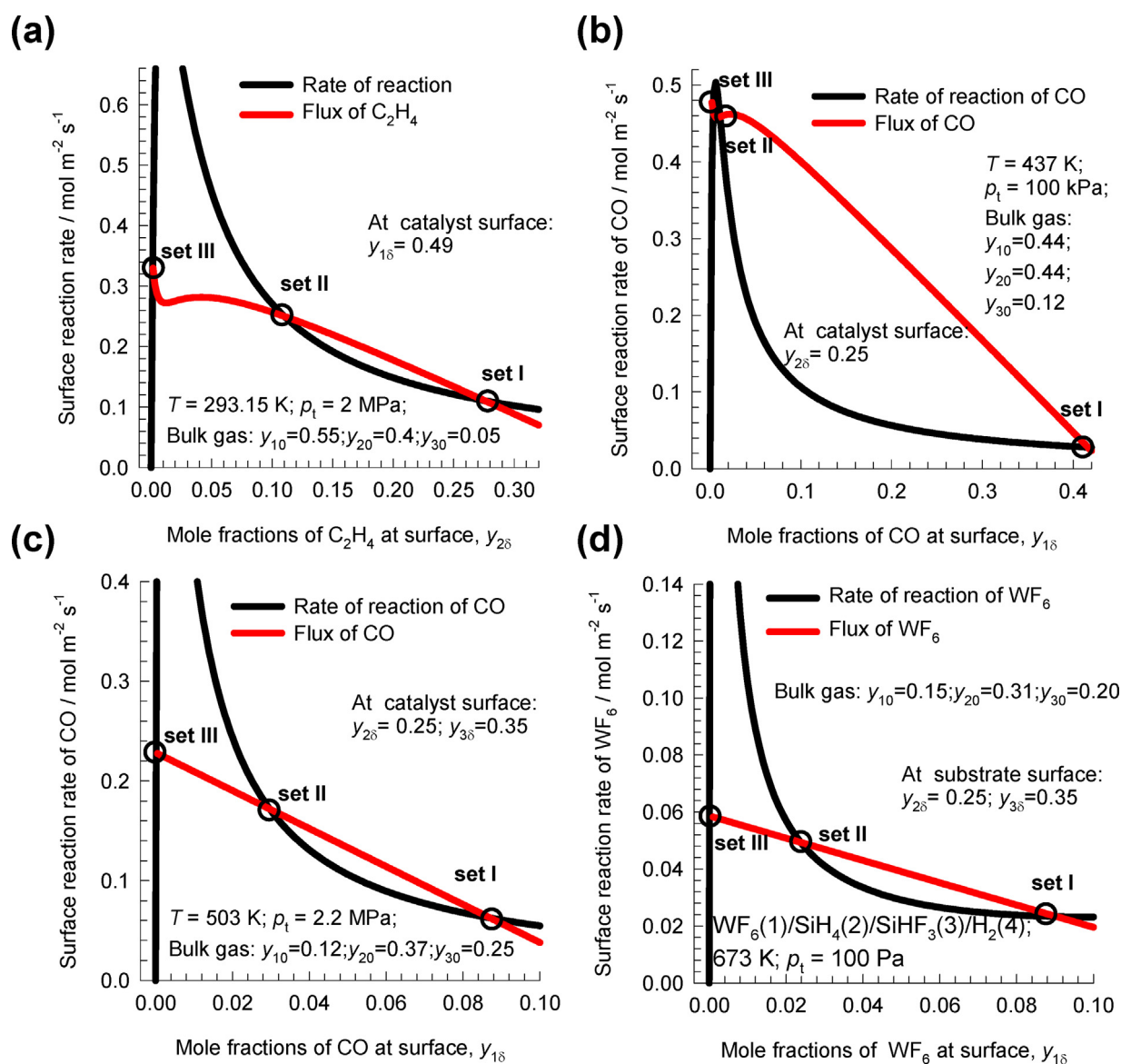
Fig. 4 – Plots of surface reaction rate and transfer flux vs surface composition of key reactant for (a) Pt/Al$_2$O$_3$ catalyzed hydrogenation ethene to produce ethane, (b) the Pt/SiO$_2$ catalyzed oxidation of CO to produce CO$_2$, (c) Ni/Al$_2$O$_3$ catalyzed methanation of CO, and (d) W deposition on Si substrate. Further calculation details are provided in Supplementary material.

linear surface kinetics expression will only yield one intersection point.

It is worth emphasizing that the observed multiplicities witnessed in the foregoing systems are for *isothermal*, *isobaric* operations; it is much more commonplace to find multiplicities for non-isothermal and adiabatic operations; some examples are listed below.

The experiments of Wedel and Luss (1984) show steady-state multiplicities for adiabatic operation of a fixed bed reactor for methanation of CO; the origins are traced to the non-linear temperature and composition dependence in the L–H kinetic description.

The existence of multiple steady states for CVD processes has been established in the experiments of Kostjuhin and Sotirchos (2002); these authors have not, however, undertaken a detailed diffusion/reaction analysis and attribute the multiplicities to "interactions of the reaction steps" in the deposition process.

Uppal and Ray (1977) have detected three different steady states for Pt/Al$_2$O$_3$ catalyzed hydrogenation of ethene, subject to *intra*-particle diffusion limitations. For non-isothermal

operations in fixed-bed catalytic hydrogenation of ethyne and ethene (Bos et al., 1993), present experimental evidence of ignition/extinction phenomena, and dynamic oscillatory behaviors arising from non-linear temperature and composition dependence of the L–H kinetics. The experiments of Herskowitz and Kenney (1983) and Oh et al. (1979) demonstrate that the Pt/SiO$_2$ catalyzed CO oxidation to CO$_2$ exhibits steady-state multiplicity; neither of these works presents a diffusion/reaction analysis to trace its origins.

5. Resolving multiplicities using the Prigogine principle

How do we determine which of the three steady-state solutions obtained for the five reaction system is the one that can be realized in practice? Löwe and Bub (1976) undertook a detailed stability analysis to conclude that solution set I in Fig. 1 is the stable one. We adopt an alternative strategy, seeking recourse to the theory of irreversible thermodynamics (Prigogine, 1961; Standart et al., 1979; Taylor and Krishna, 1993). The second law of thermodynamics dictates that the

rate of entropy production must be positive definite, $\sigma \geq 0$; a detailed derivation is provided in Supplementary material:

$$\sigma = -R \frac{N_1}{\nu_1} \sum_{i=1}^{n} \left(\frac{\nu_i}{y_i} - \nu_t \right) \frac{dy_i}{dz} \geq 0 \qquad (19)$$

where $\nu_t = \nu_1 + \nu_2 + \nu_3 + \cdots \nu_n$; the situation $\sigma = 0$ manifests at thermodynamic equilibrium. The Prigogine principle of minimum entropy production says that the steady state of an irreversible process, i.e., the state in which the thermodynamic variables are independent of the time, is characterized by a minimum value of the rate of entropy production (Prigogine, 1961). The application of this principle for resolving multiplicities in diffusion of ternary gas mixtures has been established (Krishna, 2017). The parallels and contrasts between the Lyapunov stability criterion and the Prigogine principle, as applied to stability of continuous stirred tank reactors, are discussed by Tarbell (1977).

The rates of entropy production for the sets I, II, and III of Löwe/Bub system (cf. Fig. 1) are, respectively, $\sigma = 0.362$, 0.71, and 1.41. Application of the Prigogine principle leads to the conclusion that the set I is the stable solution; this is the same conclusion drawn by Löwe and Bub (1976) using a detailed stability analysis.

For each of five reaction systems (cf. Figs. 3 and 4), the solution set I produces entropy at the minimum rate and these must correspond to the stable, physically realizable, steady-state.

6. Significance of diffusional coupling effects in CVD process

We now examine whether there is any penalty associated with assuming equal diffusivities for all the constituent binary pairs, $Đ_{ij} = Đ$ because this expediency results in a set of *uncoupled* flux Eq. (17). Fig. 5 presents the composition profiles in the gas "film" for components participating in the process of W deposition $WF_6 + 2SiH_4 \rightarrow W_{(s)} + 2SiHF_3 + 3H_2$. The profiles correspond to the two sets of stable steady state solutions (set I), calculated using the rigorous Eq. (12), and the simplified Eq. (16). In the latter case, we make the assumption $Đ = Đ_{13} = 0.013 \, \mathrm{m^2 \, s^{-1}}$, the lowest pair diffusivity in the mixture. The W deposition rates for the stable solution sets I are, respectively, $N_1 = 0.01916$, and $N_1 = 0.00763 \, \mathrm{mol \, m^{-2} \, s^{-1}}$. The large differences in the deposition rates, differing by more than a factor two, underscores the need for taking proper account of differences in the binary pair diffusivities in CVD processes; the same conclusion has been reached by Kuijlaars et al. (1995).

7. Conclusions

A combination of Maxwell–Stefan and Langmuir–Hinshelwood formulations for describing diffusion and surface reaction has been used to analyze five different reaction systems. The following major conclusions emerge from the work.

1. The effective diffusivity concept, defined in Eq. (6), is particularly convenient for diffusion/reaction systems. This concept is implementable in existing models for microchannel reactors such that of Russo et al. (2015).
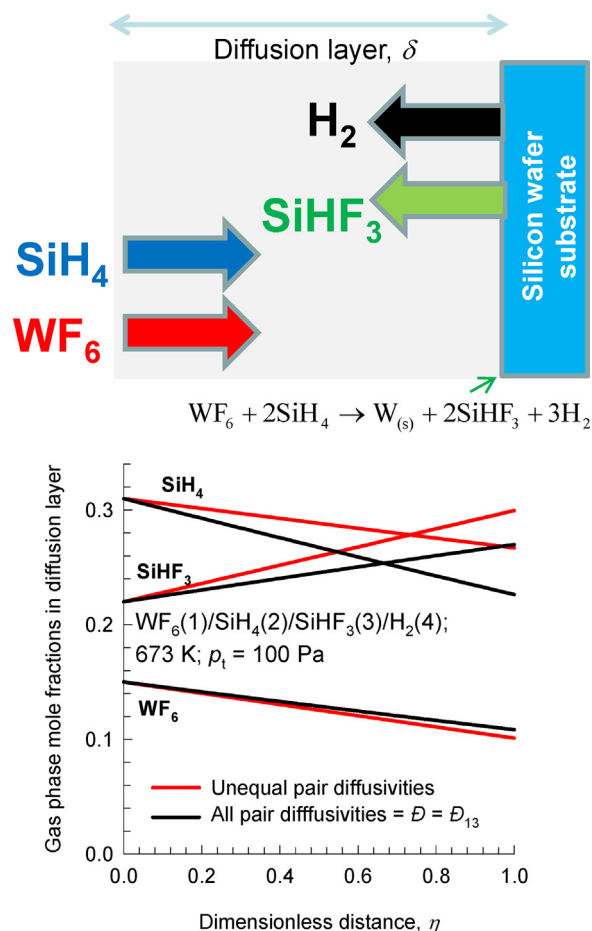

Fig. 5 – Composition profiles in the gas "film" for components participating in the process of W deposition $WF_6 + 2SiH_4 \rightarrow W_{(s)} + 2SiHF_3 + 3H_2$. The profiles correspond to the two sets of stable steady state solutions, calculated using Eqs. (12) and (16). Further calculation details are provided in Supplementary material.

2. The simultaneous solution of the analytic expression for the transfer fluxes (Eq. (15)), and the L–H expression for surface reaction (Eq. (18)) yields three different solution (sets I, II, and III) for the five reaction systems. The origin of the multiplicities is traceable to the non-linearities of L–H kinetics.

3. The Prigogine principle of minimum entropy production indicates that the low-conversion steady-state (set I) is the stable one that will be realizable in practice; its use obviates the need for undertaking a detailed stability analysis.

4. For modelling of CVD processes, it is important to take proper account of differences in the diffusivities of the constituent binary pairs in the mixture.

For reactive distillation processes, multiple steady states are routinely observed (Higler et al., 1999; Taylor and Krishna, 2000); the analysis of such phenomena requires extension of current work to include vapor/liquid phase equilibrium, and intra-catalyst diffusion. The analysis also needs to be extended to cases for which the surface chemical reactions do not obey L–H kinetics, as may be the case of CO oxidation (Temel et al., 2007).

Notation

$Đ_{ij}$ M–S binary pair diffusivity, $\mathrm{m^2 \, s^{-1}}$
$D_{i,eff}$ Effective diffusivity of component i, $\mathrm{m^2 \, s^{-1}}$

$[I]$	Identity matrix, dimensionless
k	Reaction rate constant
K	Langmuir adsorption constant, Pa^{-1}
n	Number of species in the mixture, dimensionless
N_i	Molar flux of species i, $mol\,m^{-2}\,s^{-1}$
N_t	Total molar flux of mixture, $mol\,m^{-2}\,s^{-1}$
p_i	Partial pressure of component i, Pa
p_t	Total pressure, Pa
R	Gas constant, $8.314\,J\,mol^{-1}\,K^{-1}$
T	Absolute temperature, K
y_i	Mole fraction of component i in gas phase, dimensionless
z	Direction coordinate, m

Greek letters

δ	Film thickness, m
δ_{ij}	Kronecker delta, dimensionless
η	Dimensionless distance in diffusion layer, dimensionless
ν_i	Stoichiometric reaction coefficient, dimensionless
σ	Rate of entropy production, $J\,m^{-3}\,s^{-1}\,K^{-1}$
Φ_{ij}	Dimensionless mass transfer rate factors, dimensionless
ϕ_i	Dimensionless mass transfer rate factors, dimensionless

Subscript

0	Referring to position, $z = 0$
δ	Referring to position, $z = \delta$
η	Referring to position, $z = \eta$
i	Component index

Appendix A. Supplementary data

Supplementary data associated with this article can be found, in the online version, at https://doi.org/10.1016/j.cherd.2017.10.028.

References

Ammerlaan, J.A.M., van Der Put, P.J., Schoonman, J., 1993. Kinetics of tungsten low-pressure chemical-vapor deposition using WF_6 and SiH_4 studied by *in situ* growth-rate measurements. J. Appl. Phys. 73, 4631–4636.

Bos, A.N.R., Hof, E., Kuper, W., Westerterp, K.R., 1993. The behaviour of a single catalyst pellet for the selective hydrogenation of ethyne in ethene. Chem. Eng. Sci. 48, 1959–1969.

Brooks, K.P., Hu, J., Zhu, H., Kee, R.J., 2007. Methanation of carbon dioxide by hydrogen reduction using the sabatier process in microchannel reactors. Chem. Eng. Sci. 62, 1161–1170.

Deshmukh, S.R., Tonkovich, A.L.Y., Jarosch, K.T., Schrader, L., Fitzgerald, S.P., Kilanowski, D.R., Lerou, J.J., Mazanec, T.J., 2010. Scale-up of microchannel reactors for Fischer–Tropsch synthesis. Ind. Eng. Chem. Res. 49, 10883–10888.

Fuller, E.N., Schettler, P.D., Giddings, J.C., 1966. A new method for prediction of binary gas-phase diffusion coefficients. Ind. Eng. Chem. 58, 19–27.

Gervais, T., Jensen, K.F., 2006. Mass transport and surface reactions in microfluidic systems. Chem. Eng. Sci. 61, 1102–1121.

Görke, O., Pfeifer, P., Schubert, K., 2005. Highly selective methanation by the use of a microchannel reactor. Catal. Today 110, 132–139.

Hernández Carucci, J.R., Halonen, V., Eränen, K., Wärnå, J., Ojala, S., Huuhtanen, M., Keiski, R., Salmi, T., 2010. Ethylene oxide formation in a microreactor: from qualitative kinetics to detailed modeling. Ind. Eng. Chem. Res. 49, 10897–10907.

Herskowitz, M., Kenney, C.N., 1983. CO oxidation on Pt supported catalysts. Kinetics and multiple steady states. Can. J. Chem. Eng. 61, 194–199.

Higler, A.P., Taylor, R., Krishna, R., 1999. Nonequilibrium modelling of reactive distillation: multiple steady states in MTBE synthesis. Chem. Eng. Sci. 54, 1389–1395.

Kiwi-Minsker, L., Renken, A., 2005. Microstructured reactors for catalytic reactions. Catal. Today 110, 2–14.

Kleijn, C.R., Hoogendoorn, C.J., 1991. A study of 2- and 3-D transport phenomena in horizontal chemical vapor deposition reactors. Chem. Eng. Sci. 46, 321–334.

Kostjuhin, I.M., Sotirchos, S.V., 2002. Multiplicity of steady states in the codeposition of silicon carbide and carbon. AIChE J. 48, 2910–2920.

Krishna, R., 1977. A generalized film model for mass transfer in nonideal fluid mixtures. Chem. Eng. Sci. 32, 659–667.

Krishna, R., 2015. Uphill diffusion in multicomponent mixtures. Chem. Soc. Rev. 44, 2812–2836.

Krishna, R., 2017. Highlighting multiplicity in the Gilliland solution to the Maxwell–Stefan equations describing diffusion distillation. Chem. Eng. Sci. 164, 63–70.

Krishna, R., Standart, G.L., 1976. A multicomponent film model incorporating a general matrix method of solution to the Maxwell–Stefan equations. AIChE J. 22, 383–389.

Krishna, R., van Baten, J.M., 2016. Describing diffusion in fluid mixtures at elevated pressures by combining the Maxwell–Stefan formulation with an equation of state. Chem. Eng. Sci. 153, 174–187.

Kuijlaars, K.J., Kleijn, C.R., Van Den Akker, H.E.A., 1995. Multi-component diffusion phenomena in multiple-wafer chemical vapor deposition reactors. Chem. Eng. J. 57, 127–136.

Löwe, A., Bub, G., 1976. Multiple steady states for isothermal catalytic gas–solid reactions with a positive reaction order. Chem. Eng. Sci. 31, 175–178.

Oh, S.H., Baron, K., Sloan, E.M., Hegedus, L.L., 1979. Effect of catalyst particle size in multiple steady states. J. Catal. 59, 272–277.

Pennline, H.W., Schehl, R.R., Haynes, W.P., Forney, A.J., 1981. Methanation in catalyst-sprayed tube wall reactors. Fuel Process. Technol. 4, 145–167.

Prigogine, I., 1961. Thermodynamics of Irreversible Processes. Interscience, New York, U.S.A.

PTC, 2013. MathCad 15.0. PTC Corporate Headquarters, Needham, http://www.ptc.com/, 3 November 2015.

Rajagopal, R., Rao, Y.K., 2004. Modeling of silicon vapor phase epitaxy using Stefan–Maxwell formalism. Mater. Trans. 45, 2395–2402.

Russo, V., Kilpiö, T., Hernández Carucci, J.R., Di Serio, M., Salmi, T., 2015. Modeling of microreactors for ethylene epoxidation and total oxidation. Chem. Eng. Sci. 134, 536–571.

Schmidt, S.A., Kumar, N., Reinsdorf, A., Eränen, K., Wärnå, J., Murzin, D.Y., Salmi, T., 2013. Methyl chloride synthesis over Al_2O_3 catalyst coated microstructured reactor—thermodynamics, kinetics and mass transfer. Chem. Eng. Sci. 95, 232–245.

Standart, G.L., Taylor, R., Krishna, R., 1979. The Maxwell–Stefan formulation of irreversible thermodynamics for simultaneous heat and mass transfer. Chem. Eng. Commun. 3, 277–289.

Tarbell, J.M., 1977. A thermodynamic Liapunov function for the near equilibrium CSTR. Chem. Eng. Sci. 32, 1471–1476.

Taylor, R., Krishna, R., 1993. Multicomponent Mass Transfer. John Wiley, New York.

Taylor, R., Krishna, R., 2000. Modelling reactive distillation. Chem. Eng. Sci. 55, 5183–5229.

Temel, B., Meskine, H., Reuter, K., Scheffler, M., Metiu, H., 2007. Does phenomenological kinetics provide an adequate description of heterogeneous catalytic reactions? J. Chem. Phys. 126, 204711.

Uppal, A., Ray, W.H., 1977. On the steady-state and dynamic behaviour of permeable, isothermal catalysts. Chem. Eng. Sci. 32, 649–657.

Venkataraman, K., Redenius, J.M., Schmidt, L.D., 2002. Millisecond catalytic wall reactors: dehydrogenation of ethane. Chem. Eng. Sci. 57, 2335–2343.

Wedel, S., Luss, D., 1984. Steady-state multiplicity features of an adiabatic fixed-bed reactor with Langmuir–Hinshelwood kinetics; CO or CO_2 methanation. Ind. Eng. Chem. Fundam. 23, 280–288.

Wesselingh, J.A., Krishna, R., 2000. Mass Transfer in Multicomponent Mixtures. VSSD, Delft.

Witmer, G.S., Balakotaiah, V., Luss, D., 1986. Multiplicity features of distributed systems—I: Langmuir–Hinshelwood reaction in a porous catalyst. Chem. Eng. Sci. 41, 179–186.

Yadav, R., Rinker, R.G., 1993. Steady-state methanation kinetics over a Ni/Al_2O_3 catalyst. Can. J. Chem. Eng. 71, 202–208.

Resolving Steady-State Multiplicities for Diffusion with Surface Chemical Reaction by Invoking the Prigogine Principle of Minimum Entropy Production

Rajamani Krishna

Van 't Hoff Institute for Molecular Sciences, University of Amsterdam, Science Park 904,

1098 XH Amsterdam, The Netherlands

email: r.krishna@contact.uva.nl

Table of Contents

1. Preamble

The Supplementary Material accompanying the manuscript *Resolving Steady-State Multiplicities for Diffusion with Surface Chemical Reaction by Invoking the Prigogine Principle of Minimum Entropy Production* provides (a) detailed derivation of the analytic solution to M-S equations describing diffusion with surface reaction, and (b) numerical techniques and input data used to demonstrate multiplicity of steady-states in five different reaction systems.

All the calculations and simulations presented in this article were performed using MathCad 15.[1]

For ease of reading, this document has been written as a stand-alone document. Consequently, there is some degree of overlap with the main article.

2. The Maxwell-Stefan formulation of diffusion with surface reaction

The Maxwell-Stefan diffusion equations for *n*-component ideal gas mixtures are

$$-\frac{dy_i}{dz} = \sum_{\substack{j=1 \\ j \neq i}}^{n} \frac{y_j N_i - y_i N_j}{c_t Đ_{ij}} = \sum_{\substack{j=1 \\ j \neq i}}^{n} \frac{y_j J_i - y_i J_j}{c_t Đ_{ij}}; \quad i = 1,2,\ldots n \tag{1}$$

The Onsager reciprocal relations demand the symmetry constraint $Đ_{ij} = Đ_{ji}; \quad i,j = 1,2,\ldots n$.

The molar fluxes N_i are defined in the laboratory fixed reference frame

$$N_i \equiv c_i u_i = c_t y_i u_i; \quad i = 1,2,\ldots n$$

The molar average mixture velocity u is $u = x_1 u_1 + x_2 u_2 + \cdots x_n u_n$. We also define diffusion fluxes J_i with respect to the chosen molar average reference velocity frame u:

$$J_i \equiv c_i (u_i - u); \quad i = 1,2,\ldots n$$

The diffusion fluxes J_i sum to zero

$$\sum_{i=1}^{n} J_i = \sum_{i=1}^{n} c_i u_i - \sum_{i=1}^{n} c_i u = \sum_{i=1}^{n} N_i - \sum_{i=1}^{n} c_i u = 0$$

and only n-1 of the fluxes J_i are independent. We have the inter-relation between the two fluxes

$$N_i \equiv c_i u_i = J_i + y_i N_t; \quad N_t = \sum_{i=1}^{n} N_i = c_t u$$

The M-S pair diffusivities Đ$_{ij}$ for gaseous mixtures at low pressures, below about 10 bar, can be estimated to a good level of accuracy using the Fuller-Schettler-Giddings (FSG)[2] method

$$Đ_{ij} = \frac{1.43 \times 10^{-7} T^{1.75}}{p\sqrt{M_{ij}}\left[\left(v_i^{1/3}\right)+\left(v_i^{1/3}\right)\right]^2} \quad \text{m}^2\text{s}^{-1} \text{ where } p \text{ is the pressure (expressed in bars), } M_{ij} = \frac{2}{\dfrac{1}{M_i}+\dfrac{1}{M_j}} \text{ is}$$

the mean molecular weight of the mixture (expressed in g mol^{-1}), v_i, and v_j are the diffusion volumes (expressed in cm^3 mol^{-1}) whose values are obtained by summing the contributions of the volumes of the constituent atoms in the molecular species (the values are tabulated in Table 11.1 of Reid, Prausnitz, and Poling[3]). For components encountered in CVD processes, data on diffusion volumes are provided in Table 4 of Rajagopal and Rao.[4] According to the FSG estimation procedure, the product of Đ$_{ij}$ and the total pressure, p, is a function only of temperature and is also independent of composition.

Only n-1 of the equations (1) are independent because the mole fractions sum to unity and the mole fraction gradients sum to zero $\sum_{i=1}^{n} y_i = 1; \quad \dfrac{dy_1}{dz} + \dfrac{dy_2}{dz} + ... \dfrac{dy_n}{dz} = 0$.

3. Effective diffusivity of single surface reaction

We define a dimensionless distance: $\eta = \dfrac{z}{\delta}$. The bulk vapor compositions are specified as follows

$\eta = 0; \quad z = 0; \quad (y) = (y_0)$. At the other end of the film, the boundary conditions are $\eta = 1; \quad z = \delta; \quad (y) = (y_\delta)$; at this position we have a catalytic surface with the heterogeneous reaction.

Let us first consider a single reaction system $v_1 A_1 + v_2 A_2 + v_3 A_3 + ...v_n A_n = 0$. The ratios of the fluxes N_i, in the laboratory fixed reference velocity frame, are determined by the reaction stoichiometry

and so $\dfrac{N_1}{V_1} = \dfrac{N_2}{V_2} = \dfrac{N_3}{V_3} = ... = \dfrac{N_n}{V_n}$. The total mixture flux can be expressed in terms of the flux of

component 1: $N_t = N_1\left(1 + \dfrac{V_2}{V_1} + \dfrac{V_3}{V_1} + ... + \dfrac{V_n}{V_1}\right) = \dfrac{N_1}{V_1}V_t$ where

$V_t = \left(V_1 + V_2 + V_3 + ... + V_n\right)$. The ratio of the total flux to the flux of component i is

$\dfrac{N_t}{N_i} = \dfrac{N_t}{N_1}\dfrac{N_1}{N_i} = \dfrac{V_t}{V_1}\dfrac{V_1}{V_i} = \dfrac{V_t}{V_i}$. Each of the molar fluxes N_i are related to the corresponding diffusion fluxes

J_i by $N_i = \dfrac{J_i}{\left(1 - y_i \dfrac{N_t}{N_i}\right)} = \dfrac{J_i}{\left(1 - y_i \dfrac{V_t}{V_i}\right)}$.

The "effective" diffusivities, $D_{i,\text{eff}}$ for each component i are defined as

$$N_i = -c_t D_{i,\text{eff}} \dfrac{dy_i}{dz}; \quad i = 1,2,\ldots n \tag{2}$$

Equation (1) allows us to obtain an explicit expression for the effective diffusivity of component i is

$$\dfrac{1}{D_{i,\text{eff}}} = \sum_{\substack{j=1 \\ j \neq i}}^{n} \dfrac{x_j}{Ð_{ij}}\left(1 - \dfrac{y_i N_j}{y_j N_i}\right) = \sum_{\substack{j=1 \\ j \neq i}}^{n} \dfrac{x_j}{Ð_{ij}}\left(1 - \dfrac{y_i V_j}{y_j V_i}\right); \quad i = 1,2,\ldots n \tag{3}$$

Even if the binary pair M-S diffusivites are assumed to be equal to one another, $Ð_{12} = Ð_{13} = Ð_{14} = Ð_{23} = Ð_{24} = Ð_{34} = Ð$, the M-S equations (1) simplify to

$$-\dfrac{dy_i}{dz} = \sum_{\substack{j=1 \\ j \neq i}}^{n} \dfrac{y_j N_i - y_i N_j}{c_t Ð} \tag{4}$$

It is easy to check that the effective diffusivity of all components are *not* equal to one another:

$$\dfrac{1}{D_{i,\text{eff}}} = \sum_{\substack{j=1 \\ j \neq i}}^{n} \dfrac{x_j}{Ð}\left(1 - \dfrac{y_i N_j}{y_j N_i}\right) = \sum_{\substack{j=1 \\ j \neq i}}^{n} \dfrac{x_j}{Ð}\left(1 - \dfrac{y_i V_j}{y_j V_i}\right); \quad i = 1,2,\ldots n \tag{5}$$

4. Effective diffusivity of multiple surface reactions

Let us first consider a scenario in which we have two different surface reactions taking place at $\eta = 1;\quad z = \delta;\quad (y) = (y_\delta)$. We write the two reactions as

$$V_{1,1}A_{1,1} + V_{2,1}A_{2,1} + V_{3,1}A_{3,1} + \ldots\ldots V_{n,1}A_{n,1} = 0$$
$$V_{1,2}A_{1,2} + V_{2,2}A_{2,2} + V_{3,2}A_{3,2} + \ldots\ldots V_{n,2}A_{n,2} = 0$$

Let the rates of conversion of A_1 at $\eta = 1;\quad z = \delta;\quad (y) = (y_\delta)$ for the two reactions be $Rate_{A1,1}$, and $Rate_{A1,2}$ respectively.

At steady-state the flux of A_1 is $N_1 = V_{1,1}Rate_{A1,1} + V_{1,2}Rate_{A1,2}$

The flux of A_2 is $N_2 = \dfrac{V_{2,1}}{V_{1,1}}Rate_{A1,1} + \dfrac{V_{2,2}}{V_{1,2}}Rate_{A1,2}$

The flux of A_3 is $N_3 = \dfrac{V_{3,1}}{V_{1,1}}Rate_{A1,1} + \dfrac{V_{3,2}}{V_{1,2}}Rate_{A1,2}$

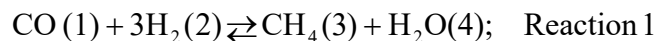The flux of A_n is $N_n = \dfrac{V_{n,1}}{V_{1,1}}Rate_{A1,1} + \dfrac{V_{n,2}}{V_{1,2}}Rate_{A1,2}$

The flux ratios are constant across the diffusion film.
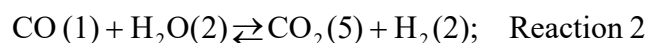
The effective diffusivity of component i is

$$\frac{1}{D_{i,eff}} = \sum_{\substack{j=1 \\ j\neq i}}^{n} \frac{x_j}{Đ_{ij}}\left(1 - \frac{y_i N_j}{y_j N_i}\right); \quad i = 1,2,\ldots n \tag{6}$$

To illustrate the calculations of the effective diffusivity using equation (6), we consider a set of two reactions at the catalyst surface:

CO methanation:

$$CO\,(1) + 3H_2\,(2) \rightleftarrows CH_4\,(3) + H_2O(4); \quad \text{Reaction 1}$$

Water gas shift reaction:

$$CO\,(1) + H_2O(2) \rightleftarrows CO_2\,(5) + H_2\,(2); \quad \text{Reaction 2}$$

The temperature is chosen as 648 K and the total pressure p_t = 2.2 MPa. Using the Fuller-Schettler-Giddings (FSG),[2] the M-S diffusivities of the constituent binary pairs are

$Đ_{12} = 14.1;\quad Đ_{13} = 3.89;\quad Đ_{14} = 4.66;\quad Đ_{15} = 2.93;$
$Đ_{23} = 12.6;\quad Đ_{24} = 16.2;\quad Đ_{25} = 11.8;$
$Đ_{34} = 4.7;\quad Đ_{35} = 3.18;$
$Đ_{45} = 3.73;$

$\times 10^{-6}$ m^2 s^{-1}. The fluxes of the five component species will be

At steady-state the flux of CO is $N_1 = Rate_{A1,1} + Rate_{A1,2}$

The flux of H$_2$ is $N_2 = 3Rate_{A1,1} - Rate_{A1,2}$

The flux of CH$_4$ is $N_3 = -Rate_{A1,1}$

The flux of H$_2$O is $N_4 = -Rate_{A1,1} + Rate_{A1,2}$

The flux of CO$_2$ is $N_5 = -Rate_{A1,2}$

Assuming that the rate of the methanation rection is twice as fast as the water gas shift reaction $Rate_{A1,1} = 2Rate_{A1,2}$, we calculate

$D_{1,eff} = 4.6;\quad D_{2,eff} = 15.7;\quad D_{3,eff} = 4.1;\quad D_{3,eff} = 4.84;\quad D_{5,eff} = 3.6 \times 10^{-6}$ m^2 s^{-1}.

5. Analytic solution to the M-S equations for steady-state transfers

For steady-state diffusion of n-component mixtures of ideal gas mixtures across a film of thickness δ, the exact analytic solution of Krishna and Standart[5] is now applied for the calculation of the fluxes.

We define a $n\text{-}1 \times n\text{-}1$ dimensional square matrix $[\Phi]$

$$\Phi_{ii} = \left(\frac{v_i}{v_1 Đ_{in}} + \sum_{k=1;k\approx i}^{k=n} \frac{v_k}{v_1 Đ_{ik}}\right)\frac{\delta}{c_t} N_1;\quad \Phi_{ik;k\neq i} = -\left(\frac{v_i}{v_1 Đ_{ik}} - \frac{v_i}{v_1 Đ_{in}}\right)\frac{\delta}{c_t} N_1;\quad i = 1,2,..n-1 \qquad (7)$$

and an n-1 dimensional column matrix (ϕ)

$$\phi_i = -\left(\frac{v_i}{v_1 Đ_{in}}\right)\frac{\delta}{c_t} N_1;\quad i = 1,2,..n-1 \qquad (8)$$

Equation (1) can be cast into n-1 dimensional matrix notation

$$\frac{d(y)}{d\eta} = [\Phi](y) + (\phi) \tag{9}$$

For steady-state transfer across a film, the matrices $[\Phi]$ and (ϕ) are both η-invariant. Therefore equation (9) represents a system of coupled *ordinary* differential equations with *constant coefficients* $[\Phi]$ and (ϕ).

The system of equations can be solved analytically to obtain the mole fraction profiles within the diffusion layer

$$(y_\eta - y_0) = -[\exp[\Phi]\eta - [I]][\exp[\Phi] - [I]]^{-1}(y_0 - y_\delta) \tag{10}$$

In equation (10), $[I]$ is the identity matrix with Kronecker delta δ_{ik} as elements.

The composition gradient at the position $\eta = \dfrac{z}{\delta}$ can be obtained by differentiation of equation (10); we get

$$\frac{d(y_\eta)}{d\eta} = -[\Phi][\exp[\Phi]\eta][\exp[\Phi] - [I]]^{-1}(y_0 - y_\delta) \tag{11}$$

The steady-state transfer fluxes of components 1,2,..n-1 can be determined from

$(N) = -\dfrac{c_t}{\delta}[D_{eff,\eta}]\dfrac{d(y_\eta)}{d\eta} = \dfrac{c_t}{\delta}[D_{eff,\eta}][\Phi][\exp[\Phi]\eta][\exp[\Phi] - [I]]^{-1}(y_0 - y_\delta)$ where the diagonal matrix of

effective diffusivities matrix at position η is $[D_{eff,\eta}]$, with elements $D_{i,eff}\delta_{ik}$, is calculated from equations (3) using the compositions at position η. Without loss of generality, we may evaluate

$[D_{eff,\eta}]$ at position $\eta = \dfrac{z}{\delta} = 0$, and obtain

$$(N) = -\frac{c_t}{\delta}\left[D_{eff,\eta=0}\right]\frac{d(y)}{d\eta}\bigg|_{\eta=0} = \frac{c_t}{\delta}\left[D_{eff,\eta=0}\right]\left[\Phi\right]\left[\exp\left[\Phi\right]-\left[I\right]\right]^{-1}(y_0 - y_\delta)$$

$$(N) = \frac{c_t}{\delta}\begin{bmatrix} D_{1,eff,\eta=0} & 0 & 0 & 0 & 0 \\ 0 & D_{2,eff,\eta=0} & 0 & 0 & 0 \\ 0 & 0 & D_{3,eff,\eta=0} & 0 & 0 \\ 0 & 0 & 0 & \ddots & 0 \\ 0 & 0 & 0 & 0 & D_{n-1,eff,\eta=0} \end{bmatrix}\left[\Phi\right]\left[\exp\left[\Phi\right]-\left[I\right]\right]^{-1}(y_0 - y_\delta) \qquad (12)$$

In Equation (12), the diagonal matrix of effective diffusivities is calculated using the compositions y_{i0} at position $\eta = \frac{z}{\delta} = 0$. Though the expression (12) appears to be explicit in the fluxes, it is to be noted that the matrix $\left[\Phi\right]\left[\exp\left[\Phi\right]-\left[I\right]\right]^{-1}$ is also a function of the fluxes.

The Sylvester's expansion formula, detailed in Equation (A.5.17) of Taylor and Krishna,[6] is required for explicit calculation of $\left[\Phi\right]\left[\exp\left[\Phi\right]-\left[I\right]\right]^{-1}$. For the n-1 dimensional matrix $\left[\Phi\right]$, the Sylvester's expansion yields

$$\left[\Phi\right]\left[\exp\left[\Phi\right]-\left[I\right]\right]^{-1} = \left(\frac{\lambda_1}{\exp(\lambda_1)-1}\right)\frac{\left[\left[\Phi\right]-\lambda_2\left[I\right]\right]}{(\lambda_1-\lambda_2)}\frac{\left[\left[\Phi\right]-\lambda_3\left[I\right]\right]}{(\lambda_1-\lambda_3)}\cdots\frac{\left[\left[\Phi\right]-\lambda_{n-1}\left[I\right]\right]}{(\lambda_1-\lambda_{n-1})} +$$

$$+ \left(\frac{\lambda_2}{\exp(\lambda_2)-1}\right)\frac{\left[\left[\Phi\right]-\lambda_1\left[I\right]\right]}{(\lambda_2-\lambda_1)}\frac{\left[\left[\Phi\right]-\lambda_3\left[I\right]\right]}{(\lambda_2-\lambda_3)}\cdots\frac{\left[\left[\Phi\right]-\lambda_{n-1}\left[I\right]\right]}{(\lambda_2-\lambda_{n-1})} +$$

$$\ldots\ldots$$

$$+ \left(\frac{\lambda_{n-1}}{\exp(\lambda_{n-1})-1}\right)\frac{\left[\left[\Phi\right]-\lambda_1\left[I\right]\right]}{(\lambda_{n-1}-\lambda_1)}\frac{\left[\left[\Phi\right]-\lambda_2\left[I\right]\right]}{(\lambda_{n-1}-\lambda_3)}\cdots\frac{\left[\left[\Phi\right]-\lambda_{n-2}\left[I\right]\right]}{(\lambda_{n-1}-\lambda_{n-1})}$$

If two eigenvalues are equal to one other, we need to use the confluent form of the Sylvester's theorem; see equation (29) of Toor.[7]

If one of the eigenvalues is zero, the application of Sylvester's theorem for evaluation of $\left[\Phi\right]\left[\exp\left[\Phi\right]-\left[I\right]\right]^{-1}$ has to be done with care, because $\frac{\lambda_i}{\exp(\lambda_i)-1}$ needs to be evaluated by use of

L'Hôpital's rule: $\frac{\lambda_i}{\exp(\lambda_i)-1} \to 1$.

For the hydrogenation reaction, $H_2 + C_2H_4 \rightleftarrows C_2H_6$, the matrix $[\Phi]$ is 2-dimensional and has two distinct eigenvalues λ_1 and λ_2. In this case, the Sylvester's formula yields

$$[\Phi][\exp[\Phi]-[I]]^{-1} = \left(\frac{\lambda_1}{\exp(\lambda_1)-1}\right)\frac{[[\Phi]-\lambda_2[I]]}{(\lambda_1-\lambda_2)} + \left(\frac{\lambda_2}{\exp(\lambda_2)-1}\right)\frac{[[\Phi]-\lambda_1[I]]}{(\lambda_2-\lambda_1)}$$

For the methanation $CO + 3H_2 \rightleftarrows CH_4 + H_2O$ reaction, the matrix $[\Phi]$ is 3-dimensional and has three distinct eigenvalues λ_1, λ_2, and λ_3. The Sylvester's expansion formula yields

$$[\Phi][\exp[\Phi]-[I]]^{-1} = \left(\frac{\lambda_1}{\exp(\lambda_1)-1}\right)\frac{[[\Phi]-\lambda_2[I]]}{(\lambda_1-\lambda_2)}\frac{[[\Phi]-\lambda_3[I]]}{(\lambda_1-\lambda_3)} +$$

$$+ \left(\frac{\lambda_2}{\exp(\lambda_2)-1}\right)\frac{[[\Phi]-\lambda_1[I]]}{(\lambda_2-\lambda_1)}\frac{[[\Phi]-\lambda_3[I]]}{(\lambda_2-\lambda_3)} +$$

$$+ \left(\frac{\lambda_3}{\exp(\lambda_3)-1}\right)\frac{[[\Phi]-\lambda_1[I]]}{(\lambda_3-\lambda_1)}\frac{[[\Phi]-\lambda_2[I]]}{(\lambda_3-\lambda_1)}$$

In the limit of vanishingly small transfer fluxes we have the limiting behavior $[\Phi][\exp[\Phi]-[I]]^{-1} \rightarrow [I]$.

Entirely analogous Sylvester's expansion formulae apply for the calculation of $[\exp[\Phi]\eta-[I]][\exp[\Phi]-[I]]^{-1}$ required in the determination of the composition profiles in the gas "film". As illustration, for 2-dimensional $[\Phi]$:

$$[\exp[\Phi]\eta-[I]][\exp[\Phi]-[I]]^{-1} = \left(\frac{\exp(\lambda_1\eta)-1}{\exp(\lambda_1)-1}\right)\frac{[[\Phi]-\lambda_2[I]]}{(\lambda_1-\lambda_2)} + \left(\frac{\exp(\lambda_2\eta)-1}{\exp(\lambda_2)-1}\right)\frac{[[\Phi]-\lambda_1[I]]}{(\lambda_2-\lambda_1)}$$

In typical practical examples, the bulk vapor compositions $\eta=0$; $z=0$; $(y)=(y_0)$ are specified or known. The n-1 independent compositions at the catalytic surface $\eta=1$; $z=\delta$; $(y)=(y_\delta)$ are all unknown. The determination of the n-1 independent compositions requires an iterative procedure in which we start by guessing the n-1 independent compositions at the catalytic surface $\eta=1$; $z=\delta$; $(y)=(y_\delta)$. The surface reaction rate, say expressed in terms of moles of component 1

converted per m^2 of surface per second, is described by the Langmuir-Hinshelwood formulation written as function of the partial pressures $p_{i\delta} = y_{i\delta} p_t$:

$$N_1 = Rate(p_{1\delta}, p_{2\delta}, ... p_{n-1,\delta}) \tag{13}$$

Since the flux ratios are fixed, there is only one unknown flux, say N_1. Insertion of equation (13) into the left member of Equations (12) results in a set of $n - 1$ independent equations in $n - 1$ unknowns

$$
\begin{pmatrix} N_1 \\ \frac{v_2}{v_1} N_1 \\ \frac{v_3}{v_1} N_1 \\ . \\ \frac{v_{n-1}}{v_1} N_1 \end{pmatrix} = \frac{c_t}{\delta} \begin{bmatrix} D_{1,eff,\eta=0} & 0 & 0 & 0 & 0 \\ 0 & D_{2,eff,\eta=0} & 0 & 0 & 0 \\ 0 & 0 & D_{3,eff,\eta=0} & 0 & 0 \\ 0 & 0 & 0 & \ddots & 0 \\ 0 & 0 & 0 & 0 & D_{n-1,eff,\eta=0} \end{bmatrix} [\Phi][\exp[\Phi] - [I]]^{-1} \begin{pmatrix} y_{10} - y_{1\delta} \\ y_{20} - y_{2\delta} \\ y_{30} - y_{3\delta} \\ . \\ y_{n-1,0} - y_{n-1.\delta} \end{pmatrix} \tag{14}
$$

In all the calculations presented in this article, we use the Given-Find solve block of MathCad 15

Equations (13) and (14), form a set of n equations that need to be solved simultaneously to determine the n unknowns (N_1, and n-1 independent compositions $y_{i\delta}$). In all the calculations presented in this article, we use the Given-Find solve block of MathCad 15 using starting guess values for n-1 independent compositions $y_{i\delta}$; this fixes the flux N_1 by invoking Equation (13).

6. Analytic solution to the M-S equations for steady-state transfers: special case of equal pair diffusivities

For the scenario in which binary pair M-S diffusivites are assumed to be equal to one another, $Đ_{12}=Đ_{13}=Đ_{14}=Đ_{23}=Đ_{24}=Đ_{34}=Đ$, the effective diffusivities are given by Equation (5). The n-1× n-1 dimensional square matrix $[\Phi]$ simplifies to the scalar quantity $\Phi = \left(1 + \sum_{k=1;k\approx i}^{k=n} \frac{v_k}{v_1}\right) \frac{\delta N_1}{c_t Đ}$. Equations (14) simplify to

$$N_i = \frac{v_i}{v_1} N_1 = \frac{c_t}{\delta} D_{i,eff,\eta=0} \frac{\Phi}{\exp(\Phi) - 1} (y_{i0} - y_{i\delta}); \quad i = 1,2,..n \tag{15}$$

The composition profiles within the diffusion gas "film" are given by the set of $n - 1$ uncoupled equations

$$y_{i\eta} = y_{i0} - \frac{\exp(\Phi\eta) - 1}{\exp(\Phi) - 1}(y_{i0} - y_{i\delta}); \quad i = 1, 2, ..n - 1 \tag{16}$$

7. Second law and the rate of entropy production

The second law of thermodynamics dictates that the rate of entropy production must be positive definite

$$\sigma = -\frac{1}{T} \sum_{i=1}^{n} \frac{d\mu_i}{dz} J_i \geq 0 \tag{17}$$

Equation (17) simplifies for ideal gas mixtures to

$$\sigma = -R \sum_{i=1}^{n} J_i \frac{1}{y_i} \frac{dy_i}{dz} \geq 0 = -R \sum_{i=1}^{n} N_i \left(1 - y_i \frac{v_t}{v_i}\right) \frac{1}{y_i} \frac{dy_i}{dz} =$$
$$= -R \sum_{i=1}^{n} N_i \left(\frac{1}{y_i} - \frac{v_t}{v_i}\right) \frac{dy_i}{dz} = -R \frac{N_1}{v_1} \sum_{i=1}^{n} \left(\frac{v_i}{y_i} - v_t\right) \frac{dy_i}{dz} \tag{18}$$

For diffusion across a film thickness δ, with boundary conditions $\begin{array}{lll} \eta = 0; & z = 0; & (y) = (y_0) \\ \eta = 1; & z = \delta; & (y) = (y_\delta) \end{array}$, the

integral average rate of entropy production can be approximated as follows

$$\sigma = \frac{R}{\delta} \frac{N_1}{v_1} \sum_{i=1}^{n} \left(\frac{v_i}{y_{i,av}} - v_t\right)(y_{i0} - y_{i\delta}) \geq 0 \tag{19}$$

In equation (19), we use the arithmetic average vapor compositions $y_{i,av} = \frac{y_{i0} + y_{i\delta}}{2}$.

8. Multiplicity of solutions in the Löwe-Bub $A_1 + 2A_2 \rightleftarrows A_3$ reaction system

We now present a re-analysis of the multiplicity in the diffusion-reaction system considered by Löwe and Bub.[8] Our objective is to demonstrate that the Prigogine principle of minimum entropy production can be gainfully employed in selecting the physically realizable, stable, solution.

The reaction scheme considered by Löwe and Bub[8] is the heterogeneous catalyzed reversible reaction

$A_1 + 2A_2 \rightleftarrows A_3$. The stoichiometric coefficients are ν_1 = 1; ν_2 = 2; ν_3 = -1. The flux ratios are

$\frac{\nu_2}{\nu_1} = 2; \frac{\nu_3}{\nu_1} = -1$. The M-S diffusivities of all species is taken to be identical to one another, and equal to $Đ$.

Even if the binary pair M-S diffusivities are equal to one another, $Đ_{12}=Đ_{13}=Đ_{23}=Đ$, it is easy to check that the effective diffusivity of all components are *not* equal to one another:

$$\frac{1}{D_{i,eff}} = \sum_{\substack{j=1 \\ j\neq i}}^{n} \frac{x_j}{Đ}\left(1 - \frac{y_i N_j}{y_j N_i}\right) = \sum_{\substack{j=1 \\ j\neq i}}^{n} \frac{x_j}{Đ}\left(1 - \frac{y_i \nu_j}{y_j \nu_i}\right); \quad i = 1,2,\ldots n$$

Equation (12) simplifies to

$$\begin{pmatrix} N_1 \\ N_2 \end{pmatrix} = \frac{c_t}{\delta}\begin{bmatrix} D_{1,eff,\eta=0} & 0 \\ 0 & D_{2,eff,\eta=0} \end{bmatrix}\begin{bmatrix} \frac{\Phi}{\exp(\Phi)-1} & 0 \\ 0 & \frac{\Phi}{\exp(\Phi)-1} \end{bmatrix}\begin{pmatrix} y_{10} - y_{1\delta} \\ y_{20} - y_{2\delta} \end{pmatrix}$$ where the dimensionless flux is

$\Phi \equiv (1 + \nu_2 + \nu_3)\frac{N_1\delta}{c_t Đ}$.

The rate of reaction, expressed as mole A (species 1) reacted per m^2 of external surface are per second

is described by the Langmuir-Hinshelwood kinetic expression $r = \frac{k_1 c_{1\delta} c_{2\delta}}{(1 + k_2 c_{1\delta} + k_3 c_{2\delta})^2}$ where

$c_{1\delta} = y_{1\delta}\frac{p_t}{RT}$ and $c_{2\delta} = y_{2\delta}\frac{p_t}{RT}$ are the molar concentrations of A (species 1) and B (species 2) at the

surface of the catalyst (position $\eta = 1;\quad z = \delta$). The total molar concentration of the gas mixture,

$$c_t = \frac{p_t}{RT}.$$

At steady-state, the flux of A (component 1) is $N_1 = \frac{c_t}{\delta} \beta_{11} \mathcal{D} \frac{\Phi}{\exp(\Phi)-1} (y_{10} - y_{1\delta}) = \frac{k_1 c_{1\delta} c_{2\delta}}{1 + k_2 c_{1\delta} + k_3 c_{2\delta}}.$

The flux of B (component 2) is $N_2 = v_2 N_1 = \frac{c_t}{\delta} \beta_{22} \mathcal{D} \frac{\Phi}{\exp(\Phi)-1} (y_{20} - y_{2\delta}).$

The flux of C (component 3) is $N_3 = v_3 N_1$. The total mixture flux $N_t = (1 + v_2 + v_3)N_1$

The diffusion fluxes are calculated from Equation (20), that simplifies to

$$J_1 = N_1 - y_1 N_t; \quad J_2 = N_2 - y_2 N_t; \quad J_3 = N_3 - y_3 N_t$$

For a specified set of bulk gas mixture compositions, y_{10} and y_{20}, there are two independent flux relations that determine the compositions, and concentrations, at the position $\eta = 1;\quad z = \delta: c_{1\delta} = y_{1\delta} c_t$ and $c_{2\delta} = y_{2\delta} c_t$. We use the Given-Find solve block of MathCad 15 to determine the unknowns $y_{1\delta}$ and $y_{2\delta}$.

Löwe and Bub[8] have demonstrated the existence of multiple steady-states by considering two different examples, Example 1, and Example 2. The diffusivity and kinetic data used Löwe and Bub[8] is presented in terms of dimensionless variables.

We shall first reproduce their published results for Example 1, for which the parameter values are

$\frac{k_1 c_t \delta}{\mathcal{D}(1 + k_3 c_t)^2} = 5.5 \times 10^{-2}; \frac{k_3}{k_2} = 10^{-3}, \frac{k_3 c_t}{1 + k_3 c_t} = 0.97$. In example 1, bulk gas composition is maintained

at $y_{10} = 0.6$, $y_{20} = 0.4$, $y_{30} = 0$.

As illustration, Figure 1 presents calculations of the dimensionless reaction rates

$\frac{k_1 c_{1\delta} c_{2\delta}}{(1 + k_2 c_{1\delta} + k_3 c_{2\delta})^2} \frac{\delta}{c_t \mathcal{D}}$, following the L-H kinetic expression used by Löwe and Bub[8] in their Example

1. The calculations. are presented for a specific choices of mole fraction of A_1 at the catalyst surface, $y_{1\delta} = 0.62$. The mole fractions of A_2 at the catalyst surface $y_{2\delta}$ are varied from 0 to 0.4. The strong

non-linear dependence of the reaction rate on the mole fraction of A_2 at the catalyst surface is evident. For the chosen bulk gas phase mole fractions $y_{10} = 0.6$, $y_{20} = 0.4$, $y_{30} = 0$, the flux of A_3 directed away the catalyst surface will decrease with increasing value of $y_{2\delta}$. Also plotted in Figure 1 are the calculations of the flux of A_3; these calculations are based on equations (15). The intersection of the two curves indicates the possible existence of three different steady-state solutions, as indicated. The intersection points serve as good starting point for determination of the precise compositions at the catalyst surface.

With the starting guesses: $y_{1\delta} = 0.62$ and $y_{2\delta} = 0.34$, $\dfrac{N_1\delta}{c_t \, \text{Đ}} = r = \dfrac{k_1 c_{1\delta} c_{2\delta}}{1 + k_2 c_{1\delta} + k_3 c_{2\delta}} = 0.08926$, we obtain

Solution set I: $\dfrac{N_1\delta}{c_t \, \text{Đ}} = 0.12103$; $y_{1\delta} = 0.62739$; $y_{2\delta} = 0.23568$; $y_{3\delta} = 0.13694$. The composition profiles, calculated using equation (10), are shown in Figure 2a. Since the composition profiles are practically linear, the rate of entropy production, Equation (18) simplifies to

$$\sigma = \frac{R}{\delta} \frac{N_1}{v_1} \left[\begin{array}{l} \left(\dfrac{v_1}{(y_{10} + y_{1\delta})/2} - v_t \right)(y_{10} - y_{1\delta}) + \left(\dfrac{v_2}{(y_{20} + y_{2\delta})/2} - v_t \right)(y_{20} - y_{2\delta}) \\[2ex] + \left(\dfrac{v_3}{(y_{30} + y_{3\delta})/2} - v_t \right)(y_{30} - y_{3\delta}) \end{array} \right] \tag{21}$$

For this solution set I, the dimensionless rate of entropy production is

$$\frac{\sigma \delta^2}{c_t \, \text{Đ} R} = \frac{R}{\delta} \frac{N_1}{v_1} \left(\frac{\delta}{c_t \, \text{Đ}} \right) \left[\begin{array}{l} \left(\dfrac{v_1}{(y_{10} + y_{1\delta})/2} - v_t \right)(y_{10} - y_{1\delta}) + \left(\dfrac{v_2}{(y_{20} + y_{2\delta})/2} - v_t \right)(y_{20} - y_{2\delta}) \\[2ex] + \left(\dfrac{v_3}{(y_{30} + y_{3\delta})/2} - v_t \right)(y_{30} - y_{3\delta}) \end{array} \right] = 0.36181.$$

With the starting guesses: $y_{1\delta} = 0.62$ and $y_{2\delta} = 0.1$, $\dfrac{N_1\delta}{c_t \, \text{Đ}} = r = \dfrac{k_1 c_{1\delta} c_{2\delta}}{1 + k_2 c_{1\delta} + k_3 c_{2\delta}} = 0.20943$, we obtain

Solution set II: $\dfrac{N_1\delta}{c_t \, \text{Đ}} = 0.18232$; $y_{1\delta} = 0.644$; $y_{2\delta} = 0.13601$; $y_{3\delta} = 0.22$. The composition profiles, calculated using equation (10), are shown in Figure 2c. For this solution set II, the dimensionless rate of entropy production is

$$\frac{\sigma\delta^2}{c_t \text{Ð} R} = \frac{R}{\delta}\frac{N_1}{v_1}\left(\frac{\delta}{c_t \text{Ð}}\right)\left[\begin{array}{l}\left(\dfrac{v_1}{(y_{10}+y_{1\delta})/2}-v_t\right)(y_{10}-y_{1\delta})+\left(\dfrac{v_2}{(y_{20}+y_{2\delta})/2}-v_t\right)(y_{20}-y_{2\delta})\\ +\left(\dfrac{v_3}{(y_{30}+y_{3\delta})/2}-v_t\right)(y_{30}-y_{3\delta})\end{array}\right] = 0.711$$

With the starting guesses: $y_{1\delta} = 0.62$ and $y_{2\delta} = 0.01$, $\dfrac{N_1\delta}{c_t \text{Ð}} = r = \dfrac{k_1 c_{1\delta} c_{2\delta}}{1+k_2 c_{1\delta}+k_3 c_{2\delta}} = 0.20995$, we obtain

Solution set III: $\dfrac{N_1\delta}{c_t \text{Ð}} = 0.24916$; $y_{1\delta} = 0.6646$; $y_{2\delta} = 0.01243$; $y_{3\delta} = 0.32298$. The composition profiles,

calculated using equation (10), are shown in Figure 2b. For this solution set III, the dimensionless rate

of entropy production is

$$\frac{\sigma\delta^2}{c_t \text{Ð} R} = \frac{R}{\delta}\frac{N_1}{v_1}\left(\frac{\delta}{c_t \text{Ð}}\right)\left[\begin{array}{l}\left(\dfrac{v_1}{(y_{10}+y_{1\delta})/2}-v_t\right)(y_{10}-y_{1\delta})+\left(\dfrac{v_2}{(y_{20}+y_{2\delta})/2}-v_t\right)(y_{20}-y_{2\delta})\\ +\left(\dfrac{v_3}{(y_{30}+y_{3\delta})/2}-v_t\right)(y_{30}-y_{3\delta})\end{array}\right] = 1.409.$$

Invoking the Prigogine principle, the stable, physically realizable, steady-state corresponds to the one

that produces entropy at the minimum rate; this implies the stable steady state solution is Solution set I:

$\dfrac{N_1\delta}{c_t \text{Ð}} = 0.12103$; $y_{1\delta} = 0.62739$; $y_{2\delta} = 0.23568$; $y_{3\delta} = 0.13694$. It is noteworthy, that Löwe and Bub[8] have

reported identical results for Solution sets I, II, and III, as should be expected. Löwe and Bub[8] present a

detailed stability analysis to reach the same conclusion that Solution set I is the stable steady-state; see

Figure 5 of their paper.

We now reproduce the results for multiplicity for Example 2 of Löwe and Bub.[8] In this case the

reaction kinetics and diffusivity data are chosen by Löwe and Bub[8] to correspond with the Eley-Rideal

reaction mechanism as described by equation (9) in the paper by Löwe and Bub.[8] The bulk phase

compositions are the same as in Example 1, i.e. $y_{10} = 0.6$, $y_{20} = 0.4$, $y_{30} = 0.0$.

Two different solutions are reported by Löwe and Bub;[8] these are referred to here as Solution set I and

Solution set II.

For Solution set I: $y_{1\delta} = 0.6414$ and $y_{2\delta} = 0.1514$, $\dfrac{N_1\delta}{c_t Đ} = 0.17331$. The composition profiles,

calculated using equation (10), are shown in Figure 3a. For this solution set I, the dimensionless rate of

entropy production is

$$\frac{\sigma\delta^2}{c_t Đ R} = \frac{R}{\delta}\frac{N_1}{v_1}\left(\frac{\delta}{c_t Đ}\right)\left[\begin{array}{l}\left(\dfrac{v_1}{(y_{10}+y_{1\delta})/2}-v_t\right)(y_{10}-y_{1\delta})+\left(\dfrac{v_2}{(y_{20}+y_{2\delta})/2}-v_t\right)(y_{20}-y_{2\delta}) \\ +\left(\dfrac{v_3}{(y_{30}+y_{3\delta})/2}-v_t\right)(y_{30}-y_{3\delta})\end{array}\right] = 0.6476$$

For Solution set II: $y_{1\delta} = 0.6555$ and $y_{2\delta} = 0.0669$, $\dfrac{N_1\delta}{c_t Đ} = 0.22078$. The composition profiles,

calculated using equation (10), are shown in Figure 3b. For this solution set II, the dimensionless rate of

entropy production is

$$\frac{\sigma\delta^2}{c_t Đ R} = \frac{R}{\delta}\frac{N_1}{v_1}\left(\frac{\delta}{c_t Đ}\right)\left[\begin{array}{l}\left(\dfrac{v_1}{(y_{10}+y_{1\delta})/2}-v_t\right)(y_{10}-y_{1\delta})+\left(\dfrac{v_2}{(y_{20}+y_{2\delta})/2}-v_t\right)(y_{20}-y_{2\delta}) \\ +\left(\dfrac{v_3}{(y_{30}+y_{3\delta})/2}-v_t\right)(y_{30}-y_{3\delta})\end{array}\right] = 1.052$$

Our contention is that the stable, physically realizable, steady-state corresponds to the one that

produces entropy at the minimum rate; this implies the realizable solution is Solution set I: $y_{1\delta} = 0.6414$

and $y_{2\delta} = 0.1514$, $\dfrac{N_1\delta}{c_t Đ} = 0.17331$. Löwe and Bub[8] present a detailed stability analysis to reach the same

conclusion that Solution set I is the stable steady-state; see Figure 4 of their paper. The use of the

Prigogine principle of minimum entropy production obviates the need for performing detailed stability

analysis to determine the stable steady-state.

9. Steady-state multiplicities for $C_2H_4 + \frac{1}{2}O_2 \rightleftarrows C_2H_4O$ reaction

For epoxidation of ethene $C_2H_4 + \frac{1}{2}O_2 \rightleftarrows C_2H_4O$ the gas phase mixture consists of three species

C_2H_4 (1), O_2 (2), and C_2H_4O (3). The molar masses of the species are, respectively: 28, 32, and 44 g

mol^{-1}. The flux ratios are $\frac{v_2}{v_1} = \frac{1}{2}; \frac{v_3}{v_1} = -1$.

Using the publications of Hernández Carucci et al.,[9] and Russo et al.[10] on epoxidation of C_2H_4 in a

micro-reactor made of pure silver, that also acts as catalyst, the temperature is chosen as 573 K and the

total pressure p_t = 200 kPa. Using the Fuller-Schettler-Giddings (FSG) estimation procedure,[2] the M-S

diffusivities of the constituent binary pairs are $Đ_{12} = 2.45; \quad Đ_{13} = 1.64; \quad Đ_{23} = 2.08 \times 10^{-5}$ m^2 s^{-1}.

Calculations of the effective diffusivities according to eq. (2) are shown in Figure 4 for conditions in

which the ratio of the compositions x_2/x_1 = 1. The effective diffusivity of C_2H_4O is about a factor 2

lower than that of O_2; this is ascribable to the fact that the transfer of C_2H_4O is in a direction opposite to

the net mixture flux $N_t = N_1 + \frac{1}{2}N_1 - N_1 = \frac{1}{2}N_1$, that is directed towards the catalyst surface.

According to the work of Russo et al.m[10] the Ag catalyzed epoxidation reaction follows Langmuir-

Hinshelwood kinetics $\frac{k_1 c_{1\delta} c_{2\delta}}{1 + K_E c_{1\delta} + K_{O2} c_{2\delta}}$ mol m^{-3} s^{-1}, where $c_{1\delta} = y_{1\delta} \frac{p_t}{RT}$ and $c_{2\delta} = y_{2\delta} \frac{p_t}{RT}$ are the

molar concentrations of C_2H_4 (1), and O_2 (2), at the surface of the catalyst (position $\eta = 1; \quad z = \delta$)

expressed in mol m^{-3}. For our calculations, we use the kinetic parameters as listed in Table 3 of Russo

et al.[10] At the chosen reaction temperature, T = 573 K, we obtain the parameter values, $k_1 = 0.7056$,

$K_E = 4.1$, and $K_{O2} = 0.316$. The rate of surface reaction, expressed as mole CO (species 1) reacted per

m^2 of external surface are per second is calculated from $Rate(c_{1\delta}, c_{2\delta}) = \frac{10^3 k_1 c_{1\delta} c_{2\delta}}{1 + K_E c_{1\delta} + K_{O2} c_{2\delta}}$ where the

factor 10^3 is used to convert to reaction rate per surface area of catalyst.

The mole fractions of C_2H_4 (1), O_2 (2), and C_2H_4O (3) in the bulk gas phase at position $\eta = 0$; $z = 0$ are chosen as $y_{10} = 0.5, y_{20} = 0.25, y_{30} = 0.25$. The total molar concentration of the gas mixture, $c_t = \dfrac{p_t}{RT} = 41.98$ mol m^{-3}, is constant across the diffusion "film", whose thickness is taken to be, $\delta = 10^{-5}$ m.

At steady-state, the flux of C_2H_4, N_1, equals the reaction rate, i.e.

$$N_1 = Rate(c_{1\delta}, c_{2\delta}) = \frac{10^3 k_1 c_{1\delta} c_{2\delta}}{1 + K_E c_{1\delta} + K_{O2} c_{2\delta}} \tag{22}$$

As illustration, Figure 5 presents calculations of the surface reaction rate using equation (22) for varying mole fraction of C_2H_4 at the catalyst surface, $y_{1\delta}$ from 0 to 0.4 while constraining the mole fraction of O_2 at the surface to $y_{2\delta} = 0.1$. The strong non-linear dependence of the reaction rate on the mole fraction of C_2H_4 at the catalyst surface is evident. For the chosen bulk gas phase mole fractions $y_{10} = 0.5, y_{20} = 0.25, y_{30} = 0.25$, the flux of C_2H_4 will be directed towards the catalyst surface; the flux will decrease with increasing values of $y_{1\delta}$. Also plotted in Figure 5 are the calculations of the flux of C_2H_4; these calculations are based on Equations (14). The intersection of the two curves indicates the possible existence of three different steady-state solutions. The intersection points serve as good starting point for determination of the precise compositions at the catalyst surface.

For a chosen bulk gas mixture composition, $y_{10} = 0.5, y_{20} = 0.25, y_{30} = 0.25$, the Given-Find solve block of MathCad 15 was used for solving the set of 2 independent Equations (14).

For the starting guess values $y_{1\delta} = 0.4; y_{2\delta} = 0.1$, and

$$N_1 = Rate(c_{1\delta}, c_{2\delta}) = \frac{10^3 k_1 c_{1\delta} c_{2\delta}}{1 + K_E c_{1\delta} + K_{O2} c_{2\delta}} = 9.8 \text{ mol m}^{-2}\text{ s}^{-1}$$ the final converged values are

$y_{1\delta} = 0.23246; y_{2\delta} = 0.14524; N_1 = 22.7$ mol m^{-2} s^{-1}. Let us term this as solution set I. The composition profiles in the "film", calculated using equation (10) are shown as the continuous red lines in Figure 6.

For this solution set I, the rate of entropy production is $\sigma = \dfrac{R}{\delta} \dfrac{N_1}{V_1} \sum\limits_{i=1}^{3} \left(\dfrac{V_i}{y_{i,av}} - V_t \right) (y_{i0} - y_{i\delta}) = 3.5 \times 10^7$ J

m^{-3} K^{-1} s^{-1}.

For the starting guess values $y_{1\delta} = 0.08; y_{2\delta} = 0.1$, and

$N_1 = Rate(c_{1\delta}, c_{2\delta}) = \dfrac{10^3 k_1 c_{1\delta} c_{2\delta}}{1 + K_E c_{1\delta} + K_{O2} c_{2\delta}} = 32.57$ mol m^{-2} s^{-1} the final converged values are

$y_{1\delta} = 0.07452; y_{2\delta} = 0.0843; N_1 = 34.7$ mol m^{-2} s^{-1}. Let us term this as solution set II. The composition

profiles in the "film", calculated using equation (10) are shown as the continuous blue lines in Figure 6.

For this solution set II, the rate of entropy production is $\sigma = \dfrac{R}{\delta} \dfrac{N_1}{V_1} \sum\limits_{i=1}^{3} \left(\dfrac{V_i}{y_{i,av}} - V_t \right) (y_{i0} - y_{i\delta}) = 8.8 \times 10^7$ J

m^{-3} K^{-1} s^{-1}.

For the starting guess values $y_{1\delta} = 0.01; y_{2\delta} = 0.1$, and

$N_1 = Rate(c_{1\delta}, c_{2\delta}) = \dfrac{10^3 k_1 c_{1\delta} c_{2\delta}}{1 + K_E c_{1\delta} + K_{O2} c_{2\delta}} = 75.9$ mol m^{-2} s^{-1} the final converged values are

$y_{1\delta} = 2.85 \times 10^{-3}; y_{2\delta} = 0.05626; N_1 = 39.9$ mol m^{-2} s^{-1}. Let us term this as solution set III. The

composition profiles in the "film", calculated using equation (10) are shown as the continuous green

lines in Figure 6. For this solution set III, the rate of entropy production is

$\sigma = \dfrac{R}{\delta} \dfrac{N_1}{V_1} \sum\limits_{i=1}^{3} \left(\dfrac{V_i}{y_{i,av}} - V_t \right) (y_{i0} - y_{i\delta}) = 12.5 \times 10^7$ J m^{-3} K^{-1} s^{-1}.

Invoking the Prigogine principle, the stable, physically realizable, steady-state corresponds to the one

that produces entropy at the minimum rate; this implies the realizable solution is Solution set I,

corresponding to the "low conversion" steady-state.

10. Steady-state multiplicities for the $CO + 3H_2 \rightleftarrows CH_4 + H_2O$ reaction

For methanation of carbon monoxide, $CO + 3H_2 \rightleftarrows CH_4 + H_2O$ the gas phase mixture consists of four species CO (1), H_2 (2), CH_4 (3), and H_2O (4). The molar masses of the four species are, respectively: 28, 2, 16.04, and 18 g mol^{-1}. The flux ratios are $\frac{v_2}{v_1} = 3; \frac{v_3}{v_1} = -1; \frac{v_4}{v_1} = -1$.

The temperature in the methanation reactor is chosen as 503 K and the total pressure p_t = 2.2 MPa. Using the Fuller-Schettler-Giddings (FSG) estimation procedure,[2] the M-S diffusivities of the constituent binary pairs are
$$\begin{aligned} Đ_{12} &= 9.04; \quad Đ_{13} = 2.5; \quad Đ_{14} = 3; \\ Đ_{23} &= 8.1; \quad Đ_{24} = 10.4; \\ Đ_{34} &= 3.022; \end{aligned}$$
$\times 10^{-6}$ m^2 s^{-1}. Calculations of the effective diffusivities according to eq. (2) are shown in Figure 7 for conditions in which the ratio of the compositions $x_2/x_1 = 3$, and $x_4/x_3 = 1$. The effective diffusivity of H_2 is about a factor 3 higher than that of CO.

For Ni/Al$_2$O$_3$ catalyst, the reaction rate $Rate(p_{1\delta}, p_{2\delta}, p_{3\delta}, p_{4\delta})$, expressed as moles of CO converted per m^2 of surface per second is calculated by the kinetic expression of Yadav and Rinker[11]:

$$Rate(p_{1\delta}, p_{2\delta}, p_{3\delta}, p_{4\delta}) = \frac{k_1 A p_{1\delta} p_{2\delta}^{0.5}}{\left[1 + B p_{1\delta} + C p_{2\delta}^{0.5} \right]^2}$$

wherein the partial pressures are expressed in kPa. The equilibrium constants have the values $A = 831.63$, $B = 354.42$, and $B = 50.57$ and the reaction rate constant has the value $k_1 = 80$, yielding the reaction rate in the units of CO converted per m^2 of surface per second. At steady-state, the flux of CO, N_1, equals the reaction rate, i.e.

$$Rate(p_{1\delta}, p_{2\delta}, p_{3\delta}, p_{4\delta}) = \frac{k_1 A p_{1\delta} p_{2\delta}^{0.5}}{\left[1 + B p_{1\delta} + C p_{2\delta}^{0.5} \right]^2} \tag{23}$$

The total molar concentration of the gas mixture, $c_t = \frac{p_t}{RT} = 526.07$ mol m^{-3}, is constant across the diffusion "film", whose thickness is taken to be, $\delta = 1$ mm.

As illustration, Figure 8 presents calculations of the surface reaction rate using equation (23) for varying mole fraction of CO at the catalyst surface, $y_{1\delta}$ from 0 to 0.1 with restraints $y_{2\delta} = 0.25$; $y_{3\delta} = 0.35$. The strong non-linear dependence of the reaction rate on the mole fraction of CO at the catalyst surface is evident. For the chosen bulk gas phase mole fractions $y_{10} = 0.12, y_{20} = 0.37, y_{30} = 0.25, y_{40} = 0.26$, the flux of CO will be directed towards the catalyst surface; the flux will decrease with increasing values of $y_{1\delta}$. Also plotted in Figure 8 are the calculations of the flux of CO; these calculations are based on Equations (14), with the simplification $[\Phi][\exp[\Phi] - [I]]^{-1} \rightarrow [I]$. The intersection of the two curves indicates the possible existence of three different steady-state solutions. The intersection points serve as good starting point for determination of the precise compositions at the catalyst surface.

For a chosen bulk gas mixture composition, $y_{10} = 0.12, y_{20} = 0.37, y_{30} = 0.25, y_{40} = 0.26$, the Given-Find solve block of MathCad 15 was used for solving the set of 3 independent Equations (14).

For the starting guess values $y_{1\delta} = 0.1; y_{2\delta} = 0.25; y_{3\delta} = 0.35$, and

$$N_1 = \frac{k_1 A p_{1\delta} p_{2\delta}^{0.5}}{\left[1 + B p_{1\delta} + C p_{2\delta}^{0.5}\right]^2} = 0.05478 \quad \text{mol m}^{-2} \text{ s}^{-1} \qquad \text{the final converged values are}$$

$y_{1\delta} = 0.07689; y_{2\delta} = 0.33129; y_{3\delta} = 0.29527; N_1 = 0.0808$ mol m^{-2} s^{-1}. Let us term this as solution set I. The composition profiles in the "film", calculated using equation (10) are shown as the red lines in Figure 9. For this solution set I, the rate of entropy production is

$$\sigma = \frac{R}{\delta} \frac{N_1}{v_1} \sum_{i=1}^{4} \left(\frac{v_i}{y_{i,av}} - v_t \right) (y_{i0} - y_{i\delta}) = 0.716 \text{ kJ m}^{-3} \text{ K}^{-1} \text{ s}^{-1}.$$

For starting guess values $y_{1\delta} = 0.04; y_{2\delta} = 0.25 \, y_{3\delta} = 0.35$, and

$$N_1 = \frac{k_1 A p_{1\delta} p_{2\delta}^{0.5}}{\left[1 + B p_{1\delta} + C p_{2\delta}^{0.5}\right]^2} = 0.13099 \text{ mol m}^{-2} \text{ s}^{-1} \qquad \text{the final converged values are}$$

$y_{1\delta} = 0.0362; y_{2\delta} = 0.29462; y_{3\delta} = 0.33811; N_1 = 0.15484$ mol m^{-2} s^{-1}. Let us term this as solution set II. The composition profiles in the "film", calculated using equation (10), are shown as blue lines in

Figure 9. For this solution set II, the rate of entropy production is

$$\sigma = \frac{R}{\delta} \frac{N_1}{v_1} \sum_{i=1}^{4} \left(\frac{v_i}{y_{i,av}} - v_t \right) (y_{i0} - y_{i\delta}) = 2.95 \ \text{kJ m}^{-1} \text{K}^{-1} \text{s}^{-1}.$$

For starting guess values $y_{1\delta} = 0.001; \ y_{2\delta} = 0.25 \ y_{3\delta} = 0.35$, and

$$N_1 = \frac{k_1 A p_{1\delta} p_{2\delta}^{0.5}}{\left[1 + B p_{1\delta} + C p_{2\delta}^{0.5} \right]^2} = 0.88746 \quad \text{mol m}^{-2} \text{s}^{-1} \quad \text{the final converged values are}$$

$y_{1\delta} = 1.05 \times 10^{-4}; \ y_{2\delta} = 0.26199; \ y_{3\delta} = 0.37621; \ N_1 = 0.2188 \quad \text{mol m}^{-2} \text{s}^{-1}$. Let us term this as solution set

III. The composition profiles in the "film", calculated using equation (10), are shown as green lines in

Figure 9. For this solution set III, the rate of entropy production is

$$\sigma = \frac{R}{\delta} \frac{N_1}{v_1} \sum_{i=1}^{4} \left(\frac{v_i}{y_{i,av}} - v_t \right) (y_{i0} - y_{i\delta}) = 6.83 \ \text{kJ m}^{-1} \text{K}^{-1} \text{s}^{-1}.$$

Invoking the Prigogine principle, the stable, physically realizable, steady-state corresponds to the one

that produces entropy at the minimum rate; this implies the realizable solution is Solution set I,

corresponding to the "low conversion" steady-state.

Multiple steady states also manifest if all the constituent M-S diffusivities are taken to be equal to one

another, $Đ = Đ_{13} = 2.5 \times 10^{-6} \ \text{m}^2 \ \text{s}^{-1}$, corresponding to the lowest pair diffusivity. In this simplified

scenario, the set of n-1 independent equations (15) need to be solved for the n-1 unknown compositions

at the catalyst surface, and equations (16) are used to calculate the composition profiles.

For the starting guess values $y_{1\delta} = 0.05; \ y_{2\delta} = 0.25; \ y_{3\delta} = 0.35$, we obtain the solution set I, with the

final converged values: $y_{1\delta} = 0.07786; \ y_{2\delta} = 0.24469; \ y_{3\delta} = 0.33317; \ N_1 = 0.06904 \quad \text{mol m}^{-2} \text{s}^{-1}$. The

composition profiles in the "film", calculated using equation (10) are shown as the red lines in Figure

10. For this solution set I, the rate of entropy production is $\sigma = \frac{R}{\delta} \frac{N_1}{v_1} \sum_{i=1}^{4} \left(\frac{v_i}{y_{i,av}} - v_t \right) (y_{i0} - y_{i\delta}) = 1.27 \ \text{kJ}$

$\text{m}^{-3} \text{K}^{-1} \text{s}^{-1}$.

For the starting guess values $y_{1\delta} = 0.04$; $y_{2\delta} = 0.25$; $y_{3\delta} = 0.35$, we obtain the solution set II, with the final converged values: $y_{1\delta} = 0.01597$; $y_{2\delta} = 0.0604$; $y_{3\delta} = 0.45533$; $N_1 = 0.15887$ mol m^{-2} s^{-1}. The composition profiles in the "film", calculated using equation (10) are shown as the blue lines in Figure 10. For this solution set II, the rate of entropy production is $\sigma = \dfrac{R}{\delta} \dfrac{N_1}{V_1} \sum_{i=1}^{4} \left(\dfrac{V_i}{y_{i,av}} - V_t \right)(y_{i0} - y_{i\delta}) = 9.2$ kJ m^{-3} K^{-1} s^{-1}.

For the starting guess values $y_{1\delta} = 0.001$; $y_{2\delta} = 0.25$; $y_{3\delta} = 0.35$, we obtain the solution set III, with the final converged values: $y_{1\delta} = 1.9 \times 10^{-5}$; $y_{2\delta} = 0.01321$; $y_{3\delta} = 0.4868$; $N_1 = 0.18015$ mol m^{-2} s^{-1}. The composition profiles in the "film", calculated using equation (10) are shown as the green lines in Figure 10. For this solution set III, the rate of entropy production is $\sigma = \dfrac{R}{\delta} \dfrac{N_1}{V_1} \sum_{i=1}^{4} \left(\dfrac{V_i}{y_{i,av}} - V_t \right)(y_{i0} - y_{i\delta}) = 13.3$ kJ m^{-3} K^{-1} s^{-1}.

11. Steady-state multiplicities for the $WF_6 + 2SiH_4 \rightarrow W_{(s)} + 2SiHF_3 + 3H_2$ reaction

In the chemical vapor deposition (CVD) process for production of tungsten by surface reaction on a Si substrate wafer,[12] $WF_6 + 2SiH_4 \rightarrow W_{(s)} + 2SiHF_3 + 3H_2$, the gas phase mixture consists of four species WF_6 (1), SiH_4 (2), $SiHF_3$ (3), and H_2 (4). The molar masses of the four species are, respectively: 297.8, 32.1, 104.1, and 2 g mol^{-1}. The flux ratios are $\dfrac{V_2}{V_1} = 2; \dfrac{V_3}{V_1} = -2; \dfrac{V_4}{V_1} = -3$.

The temperature in the CVD reactor is chosen as 673 K and the total pressure p_t = 100 Pa. Using the Fuller-Schettler-Giddings (FSG) estimation procedure,[2, 4] the M-S diffusivities of the constituent binary pairs are
$Đ_{12} = 0.026;$ $Đ_{13} = 0.013;$ $Đ_{14} = 0.152;$
$Đ_{23} = 0.031;$ $Đ_{24} = 0.24;$
$Đ_{34} = 0.172;$
m^2 s^{-1}. Calculations of the effective diffusivities according to eq. (2) are shown in Figure 11 for conditions in which the ratio of the compositions $x_2/x_1 = 2$, and $x_4/x_3 = 3/2$. The effective diffusivity of H_2 is about an order of magnitude higher than that of

WF$_6$. The large differences in the effective diffusivities of WF$_6$ (1), SiH$_4$ (2), SiHF$_3$ (3), and H$_2$ (4) have a significant influence on the composition profiles in the effective diffusion layer between the bulk gas phase and the surface of the wafer.

The reaction rate $Rate(p_{1\delta}, p_{2\delta}, p_{3\delta}, p_{4\delta})$, expressed as moles of W deposited per m^2 of surface per second is calculated by the kinetic expression of Ammerlaan et al.[12]: $Rate(p_{1\delta}, p_{2\delta}, p_{3\delta}, p_{4\delta}) = \dfrac{k_1 p_{2\delta}^2}{p_{1\delta} p_{4\delta}^3}$ wherein the partial pressures are expressed in Pa, and the reaction rate constant $k_1 = 10$, yielding the units of moles of W deposited per m^2 of surface per second. At steady-state, the flux of WF$_6$, N_1, equals the reaction rate, i.e.

$$N_1 = Rate(p_{1\delta}, p_{2\delta}, p_{3\delta}, p_{4\delta}) = \frac{k_1 p_{2\delta}^2}{p_{1\delta} p_{4\delta}^3} \tag{24}$$

The total molar concentration of the gas mixture, $c_t = \dfrac{p_t}{RT}$ = 0.01787 mol m^{-3}, is constant across the diffusion "film", whose thickness is taken to be, δ = 1 mm.

As illustration, Figure 12 presents calculations of the surface reaction rate using equation (24) for varying mole fraction of WF$_6$ at the catalyst surface, $y_{1\delta}$ from 0 to 0.1 with restraints $y_{2\delta} = 0.25$; $y_{3\delta} = 0.35$. The strong non-linear dependence of the reaction rate on the mole fraction of WF$_6$ at the catalyst surface is evident. For the chosen bulk gas phase mole fractions $y_{10} = 0.15, y_{20} = 0.31, y_{30} = 0.22, y_{40} = 0.32$, the flux of WF$_6$ will be directed towards the catalyst surface; the flux will decrease with increasing values of $y_{1\delta}$. Also plotted in Figure 12 are the calculations of the flux of WF$_6$; these calculations are based on Equations (14), with the simplification $[\Phi][\exp[\Phi] - [I]]^{-1} \to [I]$. The intersection of the two curves indicates the possible existence of three different steady-state solutions. The intersection points serve as good starting point for determination of the precise compositions at the catalyst surface.

For a chosen bulk gas mixture composition, $y_{10} = 0.15, y_{20} = 0.31, y_{30} = 0.22, y_{40} = 0.32$, the Given-Find solve block of MathCad 15 was used for solving the set of 3 independent Equations (14).

For the starting guess values $y_{1\delta} = 0.09; y_{2\delta} = 0.25; y_{3\delta} = 0.35$, and

$$N_1 = \frac{k_1 p_{2\delta}^2}{p_{1\delta} p_{4\delta}^3} = 0.02331 \text{ mol m}^{-2} \text{ s}^{-1} \qquad \text{the} \qquad \text{final} \qquad \text{converged} \qquad \text{values} \qquad \text{are}$$

$y_{1\delta} = 0.10108; y_{2\delta} = 0.2669; y_{3\delta} = 0.29949; N_1 = 0.01916 \quad \text{mol m}^{-2} \text{ s}^{-1}$. Let us term this as solution set I. The composition profiles in the "film", calculated using equation (10) are shown as the red lines in Figure 13. For this solution set I, the rate of entropy production is

$$\sigma = \frac{R}{\delta} \frac{N_1}{v_1} \sum_{i=1}^{4} \left(\frac{v_i}{y_{i,av}} - v_t \right)(y_{i0} - y_{i\delta}) = 0.226 \text{ kJ m}^{-3} \text{ K}^{-1} \text{ s}^{-1}.$$

For slightly different starting guess values $y_{1\delta} = 0.04; y_{2\delta} = 0.25; y_{3\delta} = 0.35$, and

$$N_1 = \frac{k_1 p_{2\delta}^2}{p_{1\delta} p_{4\delta}^3} = 0.03349 \text{ mol m}^{-2} \text{ s}^{-1} \qquad \text{the} \qquad \text{final} \qquad \text{converged} \qquad \text{values} \qquad \text{are}$$

$y_{1\delta} = 0.01563; y_{2\delta} = 0.19167; y_{3\delta} = 0.43835; N_1 = 0.05284 \quad \text{mol m}^{-2} \text{ s}^{-1}$. Let us term this as solution set II. The composition profiles in the "film", calculated using equation (10) are shown as blue lines in Figure 13. The composition profiles for set II are steeper than for set I. For this solution set II, the rate

of entropy production is $\sigma = \dfrac{R}{\delta} \dfrac{N_1}{v_1} \sum_{i=1}^{4} \left(\dfrac{v_i}{y_{i,av}} - v_t \right)(y_{i0} - y_{i\delta}) = 1.84 \text{ kJ m}^{-3} \text{ K}^{-1} \text{ s}^{-1}$.

We were unable to able to find the third solution set.

Invoking the Prigogine principle, the stable, physically realizable, steady-state corresponds to the one that produces entropy at the minimum rate; this implies the realizable solution is Solution set I.

Multiple steady states also manifest if all the constituent M-S diffusivities are taken to be equal to one another, $Đ = Đ_{13} = 0.013 \text{ m}^2 \text{ s}^{-1}$, corresponding to the lowest pair diffusivity. In this simplified scenario, the set of n-1 independent equations (15) need to be solved for the n-1 unknown compositions at the catalyst surface, and equations (16) are used to calculate the composition profiles.

For the starting guess values $y_{1\delta} = 0.09$; $y_{2\delta} = 0.25$; $y_{3\delta} = 0.35$, we obtain the solution set I, with the

final converged values: $y_{1\delta} = 0.10842$; $y_{2\delta} = 0.22621$; $y_{3\delta} = 0.269899$; $N_1 = 0.00763$ mol m^{-2} s^{-1}. The

composition profiles in the "film", calculated using equation (10) are shown as the red lines in Figure

14. For this solution set I, the rate of entropy production is $\sigma = \dfrac{R}{\delta} \dfrac{N_1}{v_1} \sum\limits_{i=1}^{4} \left(\dfrac{v_i}{y_{i,av}} - v_t \right)(y_{i0} - y_{i\delta}) = 0.126$

kJ m^{-3} K^{-1} s^{-1}.

For slightly different starting guess values $y_{1\delta} = 0.01$; $y_{2\delta} = 0.25$; $y_{3\delta} = 0.35$, we obtain the solution

set II, with the final converged values:

$y_{1\delta} = 9.45 \times 10^{-6}$; $y_{2\delta} = 9.45 \times 10^{-3}$; $y_{3\delta} = 0.4$; $N_1 = 0.03028$ mol m^{-2} s^{-1}. The composition profiles in the

"film", calculated using equation (10) are shown as the blue lines in Figure 14. For this solution set II,

the rate of entropy production is $\sigma = \dfrac{R}{\delta} \dfrac{N_1}{v_1} \sum\limits_{i=1}^{4} \left(\dfrac{v_i}{y_{i,av}} - v_t \right)(y_{i0} - y_{i\delta}) = 2.2$ kJ m^{-3} K^{-1} s^{-1}.

12. Steady-state multiplicities for the $H_2 + C_2H_4 \rightleftarrows C_2H_6$ reaction

For hydrogenation of ethene,[13] $H_2 + C_2H_4 \rightleftarrows C_2H_6$ the gas phase mixture consists of three species H$_2$

(1), C$_2$H$_4$ (2), and C$_2$H$_6$ (3). The molar masses of the species are, respectively: 2, 28, and 30 g mol^{-1}. The

flux ratios are $\dfrac{v_2}{v_1} = 1$; $\dfrac{v_3}{v_1} = -1$.

Following the work of Uppal and Ray,[13] the temperature in the hydrogenation reactor is chosen as

293.15 K and the total pressure p_t = 2 MPa. Using the Fuller-Schettler-Giddings (FSG) estimation

procedure,[2] the M-S diffusivities of the constituent binary pairs are

$Đ_{12} = 2.76$; $Đ_{13} = 2.63$; $Đ_{23} = 0.56 \times 10^{-6}$ m^2 s^{-1}. Calculations of the effective diffusivities according

to eq. (2) are shown in Figure 15 for conditions in which the ratio of the compositions x_2/x_1 = 1. The

effective diffusivity of H$_2$ is about a factor 5 higher than that of C$_2$H$_6$.

According to the work of Uppal and Ray,[13] the Pt/Al$_2$O$_3$ catalyzed hydrogenation reaction follows Langmuir-Hinshelwood kinetics. The rate of surface reaction, expressed as mole H$_2$ (species 1) reacted per m^2 of external surface are per second is described by the Langmuir-Hinshelwood kinetic expression

$$Rate(p_{1\delta}, p_{2\delta}, p_{3\delta}) = \frac{k_1 K_A K_B p_{1\delta} p_{2\delta}}{1 + K_A p_{1\delta} + K_B p_{2\delta}}$$ where $p_{1\delta} = y_{1\delta} p_t$ and $p_{2\delta} = y_{2\delta} p_t$ are the partial pressures of

H$_2$ (species 1) and C$_2$H$_4$ (species 2) at the surface of the catalyst (position $\eta = 1$; $z = \delta$). The total pressure of the gas mixture, p_t = 2 MPa. The mole fractions H$_2$ (1), C$_2$H$_4$ (2), and C$_2$H$_6$ (3) in the bulk gas phase at position $\eta = 0$; $z = 0$ are $y_{10} = 0.55, y_{20} = 0.4, y_{30} = 0.05$. The total molar concentration of the gas mixture, $c_t = \dfrac{p_t}{RT}$ = 820.6 mol m^{-3}, is constant across the diffusion "film", whose thickness is taken to be, δ = 1 mm. The adsorption constants are $K_A = 0.5 \times 10^{-5}$ Pa^{-1}, and $K_B = 30 \times 10^{-5}$ Pa^{-1}. The reaction rate constant $k_1 = 4$ mol m^{-2} s^{-1} for conformity with the units for fluxes.

At steady-state, the flux of H$_2$, N_1, equals the reaction rate, i.e.

$$N_1 = Rate(p_{1\delta}, p_{2\delta}, p_{3\delta}) = \frac{k_1 K_A K_B p_{1\delta} p_{2\delta}}{1 + K_A p_{1\delta} + K_B p_{2\delta}} \tag{25}$$

As illustration, Figure 16 presents calculations of the surface reaction rate using equation (25) for varying mole fraction of C$_2$H$_4$ at the catalyst surface, $y_{2\delta}$ from 0 to 0.4 while constraining the mole fraction of H$_2$ at the surface to $y_{1\delta} = 0.49$. The strong non-linear dependence of the reaction rate on the mole fraction of C$_2$H$_4$ at the catalyst surface is evident. For the chosen bulk gas phase mole fractions, $y_{10} = 0.55, y_{20} = 0.4, y_{30} = 0.05$, the flux of C$_2H_4$ will be directed towards the catalyst surface; the flux will decrease with increasing values of $y_{2\delta}$. Also plotted in Figure 16 are the calculations of the flux of C$_2$H$_4$; these calculations are based on Equations (14). The intersection of the two curves indicates the possible existence of three different steady-state solutions. The intersection points serve as good starting point for determination of the precise compositions at the catalyst surface.

For a chosen bulk gas mixture composition, $y_{10} = 0.55, y_{20} = 0.4, y_{30} = 0.05$, the Given-Find solve block of MathCad 15 was used for solving the set of 2 independent Equations (14).

For the starting guess values $y_{1\delta} = 0.49\ y_{2\delta} = 0.01$, and

$$N_1 = \frac{k_1 K_A K_B p_{1\delta} p_{2\delta}}{1 + K_A p_{1\delta} + K_B p_{2\delta}} = 0.83045 \quad \text{mol m}^{-2}\ \text{s}^{-1} \quad \text{the final converged values are}$$

$y_{1\delta} = 0.52344; y_{2\delta} = 0.26699; N_1 = 0.12109 \quad \text{mol m}^{-2}\ \text{s}^{-1}$. Let us term this as solution set I. The composition profiles in the "film", calculated using equation (10) are shown as the red lines in Figure

17. For this solution set I, the rate of entropy production is $\sigma = \dfrac{R}{\delta} \dfrac{N_1}{v_1} \sum\limits_{i=1}^{3} \left(\dfrac{v_i}{y_{i,av}} - v_t \right) (y_{i0} - y_{i\delta}) = 1.69$ kJ

m^{-3} K^{-1} s^{-1}.

For slightly different starting guess values $y_{1\delta} = 0.49; y_{2\delta} = 0.02$, and

$$N_1 = \frac{k_1 K_A K_B p_{1\delta} p_{2\delta}}{1 + K_A p_{1\delta} + K_B p_{2\delta}} = 0.73406 \quad \text{mol m}^{-2}\ \text{s}^{-1} \quad \text{the final converged values are}$$

$y_{1\delta} = 0.49314; y_{2\delta} = 0.11088; N_1 = 0.24944 \quad \text{mol m}^{-2}\ \text{s}^{-1}$. Let us term this as solution set II. The composition profiles in the "film", calculated using equation (10) are shown as blue lines in Figure 17.

For this solution set II, the rate of entropy production is $\sigma = \dfrac{R}{\delta} \dfrac{N_1}{v_1} \sum\limits_{i=1}^{3} \left(\dfrac{v_i}{y_{i,av}} - v_t \right) (y_{i0} - y_{i\delta}) = 5.8$ kJ m^{-3}

K^{-1} s^{-1}.

For slightly different starting guess values $y_{1\delta} = 0.49; y_{2\delta} = 0.009$, and

$$N_1 = \frac{k_1 K_A K_B p_{1\delta} p_{2\delta}}{1 + K_A p_{1\delta} + K_B p_{2\delta}} = 0.82888 \quad \text{mol m}^{-2}\ \text{s}^{-1} \quad \text{the final converged values are}$$

$y_{1\delta} = 0.47234; y_{2\delta} = 0.00123; N_1 = 0.33333 \quad \text{mol m}^{-2}\ \text{s}^{-1}$. Let us term this as solution set III. The composition profiles in the "film", calculated using equation (10) are shown as green lines in Figure 17.

For this solution set III, the rate of entropy production is $\sigma = \dfrac{R}{\delta} \dfrac{N_1}{v_1} \sum\limits_{i=1}^{3} \left(\dfrac{v_i}{y_{i,av}} - v_t \right) (y_{i0} - y_{i\delta}) = 10.5$ kJ

m^{-3} K^{-1} s^{-1}.

Invoking the Prigogine principle, the stable, physically realizable, steady-state corresponds to the one that produces entropy at the minimum rate; this implies the realizable solution is Solution set I, corresponding to the "low conversion" steady-state.

13. Steady-state multiplicities for the $CO + \frac{1}{2}O_2 \rightleftarrows CO_2$ reaction

For oxidation of carbon monoxide,[14] $CO + \frac{1}{2}O_2 \rightleftarrows CO_2$ the gas phase mixture consists of three species CO (1), O_2 (2), and CO_2 (3). The molar masses of the species are, respectively: 28, 32, and 44 g mol^{-1}. The flux ratios are $\frac{v_2}{v_1} = \frac{1}{2}; \frac{v_3}{v_1} = -1$.

Following the work of Herskowitz and Kenney,[14] the temperature in the oxidation reactor is chosen as 437 K and the total pressure p_t = 100 kPa. Using the Fuller-Schettler-Giddings (FSG) estimation procedure,[2] the M-S diffusivities of the constituent binary pairs are $Đ_{12} = 4.11$; $Đ_{13} = 3.24$; $Đ_{23} = 3.2$ $\times 10^{-5}$ m^2 s^{-1}. Calculations of the effective diffusivities according to eq. (2) are shown in Figure 18 for conditions in which the ratio of the compositions x_2/x_1 = 1. The effective diffusivity of CO_2 is about a factor 1.5 lower than that of O_2.

According to the work of Herskowitz and Kenney,[14] the Pt/SiO$_2$ catalyzed oxidation reaction follows Langmuir-Hinshelwood kinetics. For our calculations, we use their Model I, with parameters listed in Table 2 of Herskowitz and Kenney.[14] The rate of surface reaction, expressed as mole CO (species 1) reacted per m^2 of external surface are per second is described by the Langmuir-Hinshelwood kinetic expression $Rate(c_{1\delta}, c_{2\delta}) = \frac{k_f K_{CO} c_{1\delta} \sqrt{K_{O2}} \sqrt{c_{2\delta}}}{1 + K_{CO} c_{1\delta} + \sqrt{K_{O2}} \sqrt{c_{2\delta}}}$ where $c_{1\delta} = y_{1\delta} \frac{p_t}{RT} \frac{1}{1000}$ and $c_{2\delta} = y_{2\delta} \frac{p_t}{RT} \frac{1}{1000}$

are the molar concentrations of CO (1), and O$_2$ (2), at the surface of the catalyst (position $\eta = 1$; $z = \delta$) expressed in kmol m^{-3}.

The mole fractions of CO (1), O_2 (2), and CO_2 (3) in the bulk gas phase at position $\eta = 0;\quad z = 0$ are

chosen as $y_{10} = 0.44, y_{20} = 0.44, y_{30} = 0.12$. The total molar concentration of the gas mixture, $c_t = \dfrac{p_t}{RT}$

$= 27.51$ mol m^{-3}, is constant across the diffusion "film", whose thickness is taken to be, $\delta = 1$ mm. The

adsorption constants are $K_A = 6.13 \times 10^3$ kmol^{-1} m^3 and $K_B = 1.38 \times 10^{-5}$ kmol^{-1} m^3. The reaction rate

constant $k_f = 6.527 \times 10^3$ mol m^{-2} s^{-1} for conformity with the units for the fluxes.

At steady-state, the flux of CO, N_1, equals the reaction rate, i.e.

$$N_1 = Rate(c_{1\delta}, c_{2\delta}) = \frac{k_f K_{CO} c_{1\delta} \sqrt{K_{O2}} \sqrt{c_{2\delta}}}{1 + K_{CO} c_{1\delta} + \sqrt{K_{O2}} \sqrt{c_{2\delta}}} \tag{26}$$

As illustration, Figure 19 presents calculations of the surface reaction rate using equation (26) for

varying mole fraction of CO at the catalyst surface, $y_{2\delta}$ from 0 to 0.42 while constraining the mole

fraction of O_2 at the surface to $y_{2\delta} = 0.25$. The strong non-linear dependence of the reaction rate on the

mole fraction of C_2H_4 at the catalyst surface is evident. For the chosen bulk gas phase mole fractions,

$y_{10} = 0.44, y_{20} = 0.44, y_{30} = 0.12$, the flux of CO will be directed towards the catalyst surface; the flux

will decrease with increasing values of $y_{2\delta}$. Also plotted in Figure 19 are the calculations of the flux of

CO; these calculations are based on Equations (14). The intersection of the two curves indicates the

possible existence of three different steady-state solutions. The intersection points serve as good

starting point for determination of the precise compositions at the catalyst surface for the three steady-

states.

For a chosen bulk gas mixture composition, $y_{10} = 0.44, y_{20} = 0.44, y_{30} = 0.12$, the Given-Find solve

block of MathCad 15 was used for solving the set of 2 independent Equations (14).

For   the   starting   guess   values $y_{1\delta} = 0.1\ y_{2\delta} = 0.22$,   and

$N_1 = \dfrac{k_f K_{CO} c_{1\delta} \sqrt{K_{O2}} \sqrt{c_{2\delta}}}{1 + K_{CO} c_{1\delta} + \sqrt{K_{O2}} \sqrt{c_{2\delta}}} = 0.09994$ mol m^{-2} s^{-1} the   final   converged   values   are

$y_{1\delta} = 0.40918; y_{2\delta} = 0.42606; N_1 = 0.03706$ mol m^{-2} s^{-1}. Let us term this as solution set I. The composition profiles in the "film", calculated using equation (10) are shown as the continuous red lines in Figure 20. For this solution set I, the rate of entropy production is

$$\sigma = \frac{R}{\delta} \frac{N_1}{v_1} \sum_{i=1}^{3} \left(\frac{v_i}{y_{i,av}} - v_t \right) (y_{i0} - y_{i\delta}) = 0.124 \text{ kJ m}^{-3} \text{ K}^{-1} \text{ s}^{-1}.$$

For different starting guess values $y_{1\delta} = 0.01; y_{2\delta} = 0.22$, and

$$N_1 = \frac{k_f K_{CO} c_{1\delta} \sqrt{K_{O2}} \sqrt{c_{2\delta}}}{1 + K_{CO} c_{1\delta} + \sqrt{K_{O2}} \sqrt{c_{2\delta}}} = 0.44194 \text{ mol m}^{-2} \text{ s}^{-1}$$ the final converged values are

$y_{1\delta} = 0.01057; y_{2\delta} = 0.244; N_1 = 0.45858$ mol m^{-2} s^{-1}. Let us term this as solution set II. The composition profiles in the "film", calculated using equation (10) are shown as blue lines in Figure 20.

For this solution set II, the rate of entropy production is $\sigma = \frac{R}{\delta} \frac{N_1}{v_1} \sum_{i=1}^{3} \left(\frac{v_i}{y_{i,av}} - v_t \right) (y_{i0} - y_{i\delta}) = 13.9$ kJ m^{-3} K^{-1} s^{-1}.

For different starting guess values $y_{1\delta} = 0.001; y_{2\delta} = 0.22$, and

$$N_1 = \frac{k_f K_{CO} c_{1\delta} \sqrt{K_{O2}} \sqrt{c_{2\delta}}}{1 + K_{CO} c_{1\delta} + \sqrt{K_{O2}} \sqrt{c_{2\delta}}} = 0.23363 \text{ mol m}^{-2} \text{ s}^{-1}$$ the final converged values are

$y_{1\delta} = 3.6 \times 10^{-3}; y_{2\delta} = 0.24079; N_1 = 0.46514$ mol m^{-2} s^{-1}. Let us term this as solution set III. The composition profiles in the "film", calculated using equation (10) are shown as green lines in Figure 20.

For this solution set III, the rate of entropy production is $\sigma = \frac{R}{\delta} \frac{N_1}{v_1} \sum_{i=1}^{3} \left(\frac{v_i}{y_{i,av}} - v_t \right) (y_{i0} - y_{i\delta}) = 14.4$ kJ m^{-3} K^{-1} s^{-1}.

The composition profiles for sets II and III are practically indistinguishable from each other.

Invoking the Prigogine principle, the stable, physically realizable, steady-state corresponds to the one that produces entropy at the minimum rate; this implies the realizable solution is Solution set I, corresponding to the "low conversion" steady-state.

14. Notation

a catalyst surface area per m^3, m^2 m^{-3}

c_i molar concentration of component i, mol m^{-3}

c_t total molar concentration of mixture, mol m^{-3}

$Đ_{ij}$ M-S binary pair diffusivity, m^2 s^{-1}

$D_{i,eff,}$ effective diffusivity of component i, m^2 s^{-1}

$[I]$ Identity matrix, dimensionless

J_i molar diffusion flux of species i with respect to u , mol m^{-2} s^{-1}

k reaction rate constant

K adsorption constant

M_i molar mass of species i, kg mol^{-1}

n number of species in the mixture, dimensionless

N_i molar flux of species i, mol m^{-2} s^{-1}

N_t total molar flux of mixture, mol m^{-2} s^{-1}

p_i partial pressure of component i,, Pa

p_t total pressure, Pa

R gas constant, 8.314 J mol^{-1} K^{-1}

T absolute temperature, K

y_i mole fraction of component i in gas phase, dimensionless

u molar average mixture velocity, m s^{-1}

z direction coordinate, m

Greek letters

δ film thickness, m

δ_{ij} Kronecker delta, dimensionless

η dimensionless distance in diffusion layer, dimensionless

λ_i	eigenvalues of $[\Phi]$, dimensionless
μ_i	molar chemical potential of component i, J mol^{-1}
v_i	stoichiometric reaction coefficient, dimensionless
σ	rate of entropy production, J m^{-3} s^{-1} K^{-1}
Φ_{ij}	dimensionless mass transfer rate factors, dimensionless
ϕ_i	dimensionless mass transfer rate factors, dimensionless

Subscript

0	Referring to position, $z = 0$
δ	Referring to position, $z = \delta$
η	Referring to position, $z = \eta$
i	Component index
k	Component index

15.   References

(1) PTC MathCad 15.0. http://www.ptc.com/, PTC Corporate Headquarters, Needham, 3 November 2015.

(2) Fuller, E. N.; Schettler, P. D.; Giddings, J. C. A New Method for Prediction of Binary Gas-phase Diffusion Coefficients. *Ind. Eng. Chem.* **1966**, *58*, 19-27.

(3) Reid, R.C.; Prausnitz, J. M.; Poling, B. E. *The Properties of Gases and Liquids*; 4th Edition, McGraw-Hill: New York, 1986.

(4) Rajagopal, R.; Rao, Y. K. Modeling of Silicon Vapor Phase Epitaxy Using Stefan-Maxwell Formalism. *Mater. Trans.* **2004**, *45*, 2395-2402.

(5) Krishna, R.; Standart, G. L. A multicomponent film model incorporating a general matrix method of solution to the Maxwell-Stefan equations. *A.I.Ch.E.J.* **1976**, *22*, 383-389.

(6) Taylor, R.; Krishna, R. *Multicomponent mass transfer*; John Wiley: New York, 1993.

(7) Toor, H. L. Solution of the Linearised Equations of Multi-component Mass Transfer: II. Matrix Methods. *A.I.Ch.E.J.* **1964**, *10*, 460-465.

(8) Löwe, A.; Bub, G. Multiple Steady States for Isothermal Catalytic Gas-Solid Reactions with a Positive Reaction Order. *Chem. Eng. Sci.* **1976**, *31*, 175-178.

(9) Hernández Carucci, J. R.; Halonen, V.; Eränen, K.; Wärnå, J.; Ojala, S.; Huuhtanen, M.; Keiski, R.; Salmi, T. Ethylene Oxide Formation in a Microreactor: From Qualitative Kinetics to Detailed Modeling. *Ind. Eng. Chem. Res.* **2010**, *49*, 10897-10907.

(10) Russo, V.; Kilpiö, T.; Hernández Carucci, J. R.; Di Serio, M.; Salmi, T. Modeling of Microreactors for Ethylene Epoxidation and Total Oxidation. *Chem. Eng. Sci.* **2015**, *134*, 536-571.

(11) Yadav, R.; Rinker, R. G. Steady-State Methanation Kinetics over a Ni/Al_2O_3 catalyst. *Can. J. Chem. Eng.* **1993**, *71*, 202-208.

(12) Ammerlaan, J. A. M.; van Der Put, P. J.; Schoonman, J. Kinetics of Tungsten Low-Pressure Chemical-Vapor Deposition using WF_6 and SiH_4 studied by *in situ* Growth-Rate Measurements. *J. Appl. Phys.* **1993**, *73*, 4631-4636.

(13) Uppal, A.; Ray, W. H. On the Steady-State and Dynamic Behaviour of Permeable, Isothermal Catalysts. *Chem. Eng. Sci.* **1977**, *32*, 649-657.

(14) Herskowitz, M.; Kenney, C. N. CO Oxidation on Pt Supported Catalysts. Kinetics and Multiple Steady States. *Can. J. Chem. Eng.* **1983**, *61*, 194-`199.

16. Caption for Figures

Figure 1. Calculations of the dimensionless reaction rates $\dfrac{k_1 c_{1\delta} c_{2\delta}}{\left(1 + k_2 c_{1\delta} + k_3 c_{2\delta}\right)^2} \dfrac{\delta}{c_t Ð}$, following the L-H

kinetic expression used by Löwe and Bub[8] in their Example 1. The parameters used are

$\dfrac{k_1 c_t \delta}{Ð\left(1 + k_3 c_t\right)^2} = 5.5 \times 10^{-2}$; $\dfrac{k_3}{k_2} = 10^{-3}$; $\dfrac{k_3 c_t}{1 + k_3 c_t} = 0.97$. The calculations are presented for mole fraction of

A_1 at the catalyst surface fixed at the value $y_{1\delta} = 0.62$. The mole fractions of A_2 at the catalyst surface

are varied from 0 to 0.4. Also plotted in red line is the flux of A_3 directed away from the catalyst.

Figure 2. Composition profiles in the gas film external to the catalyst surface with heterogeneous

chemical reaction $A_1 + 2A_2 \rightleftarrows A_3$. The red, blue, and green lines are the composition profiles,

calculated using equations (10), for the solution sets I, II, and III for Example 1 of Löwe and Bub.[8]

Figure 3. Composition profiles in the gas film external to the catalyst surface with heterogeneous

chemical reaction $A_1 + 2A_2 \rightleftarrows A_3$. The red, and blue lines are the composition profiles for the solution

sets I, and II for Example 2 of Löwe and Bub.[8]

Figure 4. Calculation of the effective diffusivities of the three species C_2H_4 (1), O_2 (2), and C_2H_4O (3)

participating in the surface reaction $C_2H_4 + \frac{1}{2}O_2 \rightleftarrows C_2H_4O$ at a temperature of 573 K and the total

pressure $p_t = 200$ kPa. In these calculations, the ratio of the compositions $x_2/x_1 = 1$.

Figure 5. Plot of the rate of reaction $C_2H_4 + \frac{1}{2}O_2 \rightleftarrows C_2H_4O$ and flux of C_2H_4 versus the mole fraction

of C_2H_4 at the catalyst surface, $y_{1\delta}$, with the restraint $y_{2\delta} = 0.1$.

Figure 6. Calculation of the composition profiles in the gas "film" in the gaseous mixture C_2H_4 (1), O_2

(2), and C_2H_4O (3) participating in the surface reaction $C_2H_4 + \frac{1}{2}O_2 \rightleftarrows C_2H_4O$ at a temperature of 573

K and the total pressure $p_t = 200$ kPa. The red, blue, and green lines are the composition profiles,

calculated using equations (10), for the solution sets I, II, and III.

Figure 7. Calculation of the effective diffusivities of the four species CO (1), H_2 (2), CH_4 (3), and H_2O

(4) participating in the surface reaction $CO + 3H_2 \rightleftarrows CH_4 + H_2O$ at a temperature of 503 K and total

pressure 2.2 MPa. In these calculations, the ratio of the compositions $x_2/x_1 = 3$, and $x_4/x_3 = 1$.

Figure 8. Plot of the rate of reaction $CO + 3H_2 \rightleftarrows CH_4 + H_2O$ and flux of CO versus the mole fraction of CO at the catalyst surface, with restraints $y_{2\delta} = 0.25;\quad y_{3\delta} = 0.35$.

Figure 9. Calculation of the composition profiles in the gas "film" in the gaseous mixture CO (1), H_2 (2), CH_4 (3), and H_2O (4) participating in the surface reaction $CO + 3H_2 \rightleftarrows CH_4 + H_2O$ at a temperature of 503 K and total pressure 2.2 MPa. The red, blue, and green lines are the composition profiles, calculated using equations (10), for the solution sets I, II, and III.
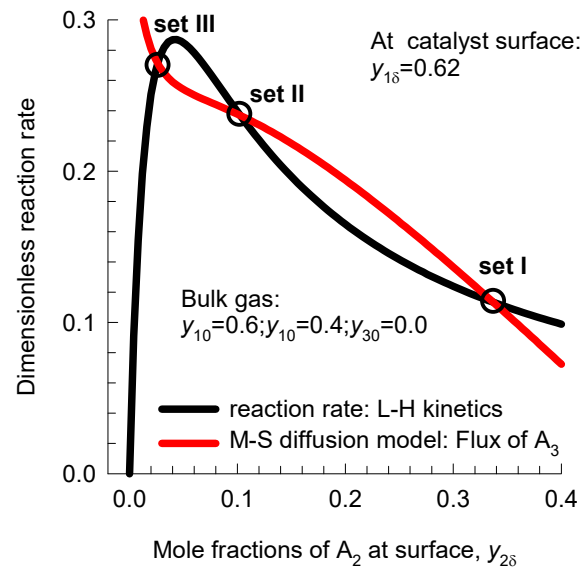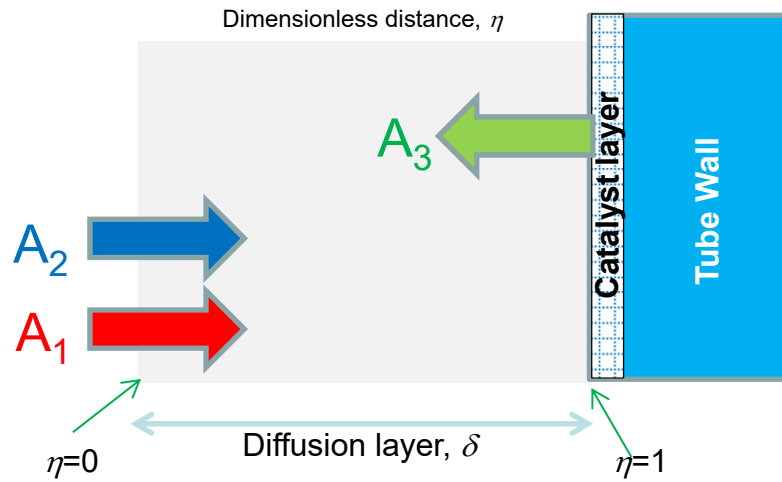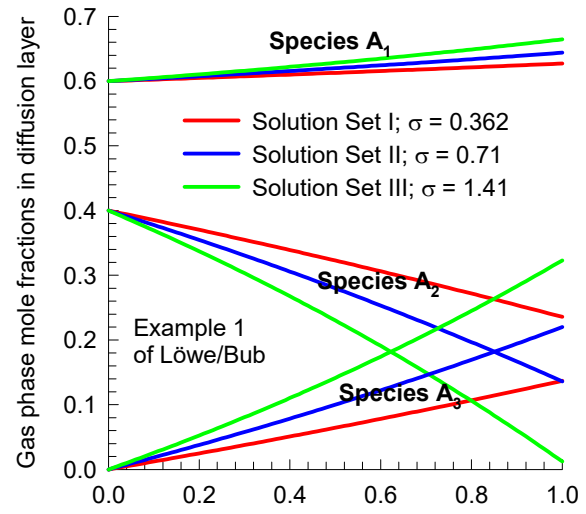
Figure 10. Calculation of the composition profiles in the gas "film" in the gaseous mixture CO (1), H_2 (2), CH_4 (3), and H_2O (4) participating in the surface reaction $CO + 3H_2 \rightleftarrows CH_4 + H_2O$ at a temperature of 503 K and total pressure 2.2 MPa. The calculations are based on Equation (16); all pair diffusivities are taken to be equal, $Đ = Đ_{13}$. The red, blue, and green lines are the composition profiles, calculated using equations (16), for the solution sets I, II, and III.

Figure 11. Calculation of the effective diffusivities of the four species WF_6 (1), SiH_4 (2), $SiHF_3$ (3), and H_2 (4) participating in the surface reaction $WF_6 + 2SiH_4 \rightarrow W_{(s)} + 2SiHF_3 + 3H_2$ at a temperature of 673 K and total pressure 100 Pa. In these calculations, the ratio of the compositions $x_2/x_1 = 2$, and $x_4/x_3 = 3/2$.

Figure 12. Plot of the rate of reaction $WF_6 + 2SiH_4 \rightarrow W_{(s)} + 2SiHF_3 + 3H_2$ and flux of WF_6 versus the mole fraction of WF_6 at the Si substrate surface, with restraints $y_{2\delta} = 0.25;\ y_{3\delta} = 0.35$.

Figure 13. Calculation of the composition profiles in the gas "film" in the gaseous mixture WF_6 (1), SiH_4 (2), $SiHF_3$ (3), and H_2 (4) participating in the surface reaction $WF_6 + 2SiH_4 \rightarrow W_{(s)} + 2SiHF_3 + 3H_2$ at a temperature of 673 K and total pressure 100 Pa. The red, blue, and green lines are the composition profiles, calculated using equations (10), for the solution sets I, II, and III.

Figure 14. Calculation of the composition profiles in the gas "film" in the gaseous mixture WF_6 (1), SiH_4 (2), $SiHF_3$ (3), and H_2 (4) participating in the surface reaction $WF_6 + 2SiH_4 \rightarrow W_{(s)} + 2SiHF_3 + 3H_2$ at a temperature of 673 K and total pressure 100 Pa. The calculations are based on Equation (16); all pair diffusivities are taken to be equal, $Đ = Đ_{13}$. The red, and blue lines are the composition profiles for the solution sets I, and II.

Figure 15. Calculation of the effective diffusivities of the three species H_2 (1), C_2H_4 (2), and C_2H_6 (3) participating in the surface reaction $H_2 + C_2H_4 \rightleftarrows C_2H_6$ at a temperature of 293.15 K and total pressure 2 MPa. In these calculations, the ratio of the compositions $x_2/x_1 = 1$.

Figure 16. Plot of the rate of $H_2 + C_2H_4 \rightleftarrows C_2H_6$ and flux of C_2H_4 versus the mole fraction of C_2H_4 at the catalyst surface, with restraint $y_{1\delta} = 0.49$.
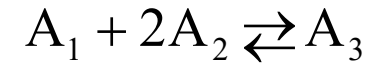
Figure 17. Calculation of the composition profiles in the gas "film" in the gaseous mixture H_2 (1), C_2H_4 (2), and C_2H_6 (3) participating in the surface reaction $H_2 + C_2H_4 \rightleftarrows C_2H_6$ at a temperature of 293.15 K and total pressure 2 MPa. The red, blue, and green lines are the composition profiles, calculated using equations (10), for the solution sets I, II, and III.

Figure 18. Calculation of the effective diffusivities of the three species CO (1), O_2 (2), and CO_2 (3) participating in the surface reaction $CO + \frac{1}{2} O_2 \rightleftarrows CO_2$ at a temperature of 437 K and the total pressure $p_t = 100$ kPa. In these calculations, the ratio of the compositions $x_2/x_1 = 1$.

Figure 19. Plot of the rate of reaction $CO + \frac{1}{2} O_2 \rightleftarrows CO_2$ and flux of CO versus the mole fraction of CO at the catalyst surface, with restraint $y_{2\delta} = 0.25$.

Figure 20. Calculation of the composition profiles in the gas "film" in the gaseous mixture CO (1), O_2 (2), and CO_2 (3) participating in the surface reaction $CO + \dfrac{1}{2}O_2 \rightleftarrows CO_2$ at a temperature of 437 K and the total pressure p_t = 100 kPa. The red, blue, and green lines are the composition profiles, calculated using equations (10), for the solution sets I, II, and III.

Surface reaction rate and flux for Löwe-Bub Example 1

At catalyst surface:
$y_{1\delta}=0.62$

Bulk gas:
$y_{10}=0.6; y_{10}=0.4; y_{30}=0.0$

set III
set II
set I

— reaction rate: L-H kinetics
— M-S diffusion model: Flux of A_3

Dimensionless reaction rate

Mole fractions of A_2 at surface, $y_{2\delta}$

Composition profiles in Löwe-Bub Example 1

$$A_1 + 2A_2 \rightleftarrows A_3$$

Species A_1

Solution Set I; $\sigma = 0.362$
Solution Set II; $\sigma = 0.71$
Solution Set III; $\sigma = 1.41$

Species A_2

Example 1
of Löwe/Bub

Species A_3

Gas phase mole fractions in diffusion layer

Dimensionless distance, η

A_3

A_2

A_1

Catalyst layer

Tube Wall

$\eta=0$

Diffusion layer, δ

$\eta=1$

Composition profiles in Löwe-Bub Example 2

Fig. 83

$$A_1 + 2A_2 \rightleftarrows A_3$$
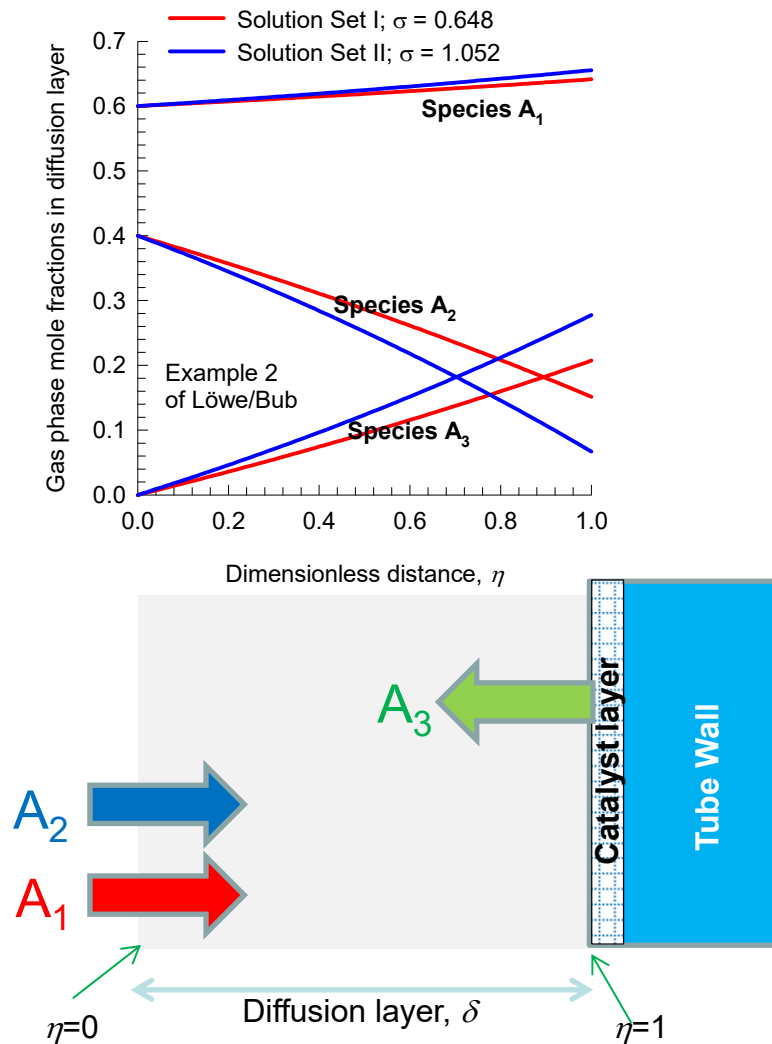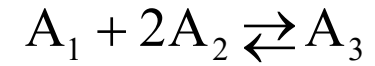
Effective Diffusivities: C$_2$H$_4$ epoxidation reaction
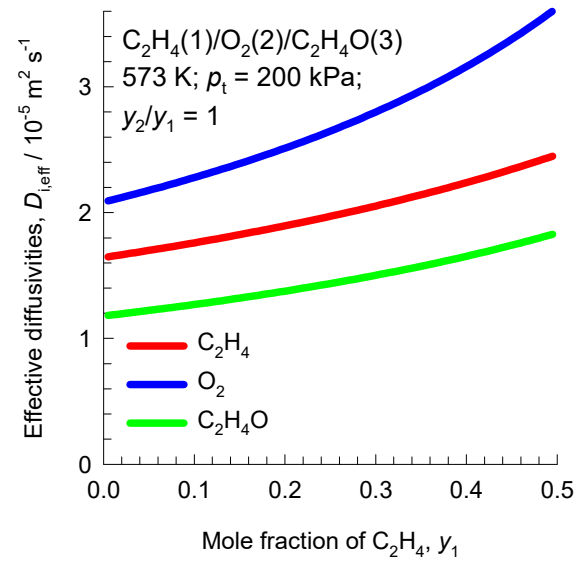
Surface reaction rate and flux for C_2H_4 epoxidation reaction
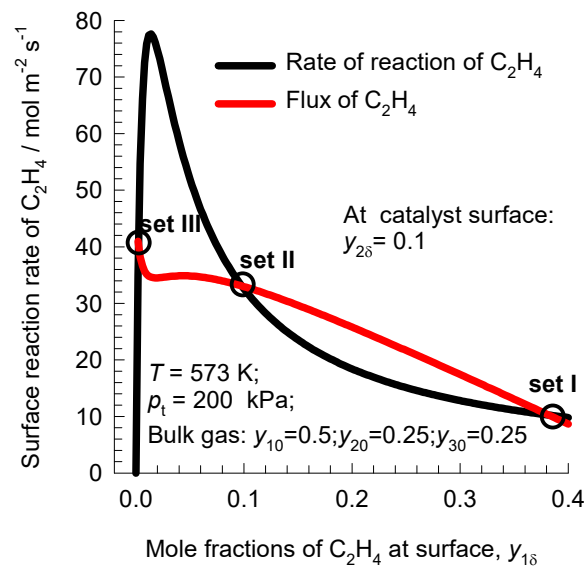
Composition profiles in "Film" Ethene epoxidation reaction
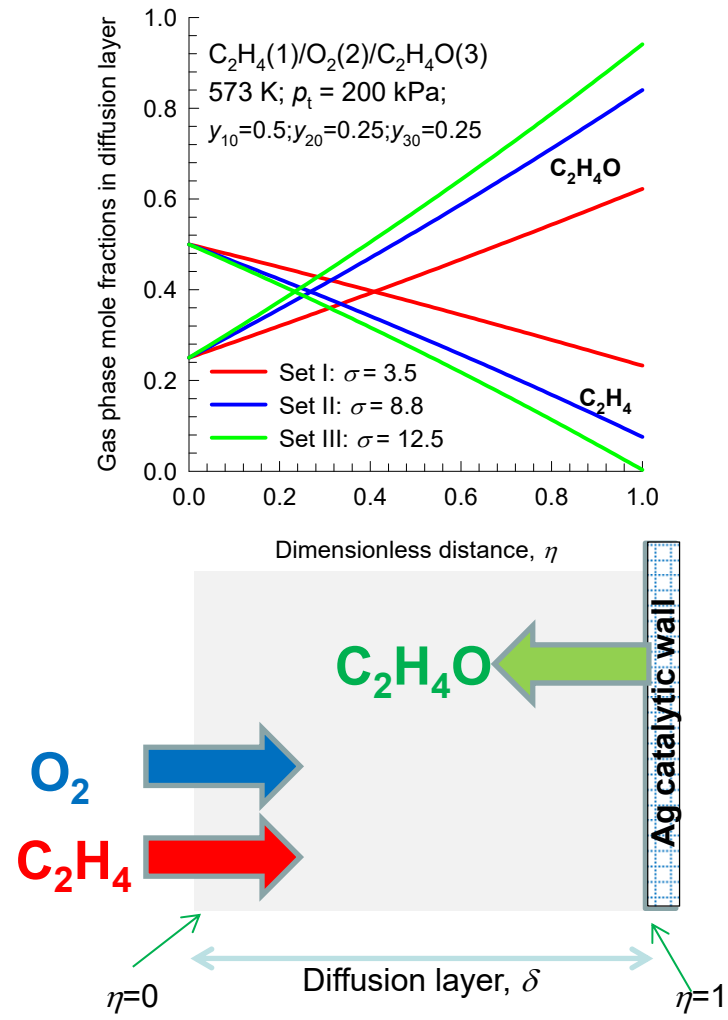
Effective diffusivities in methanation reaction

$$CO + 3H_2 \rightleftarrows CH_4 + H_2O$$
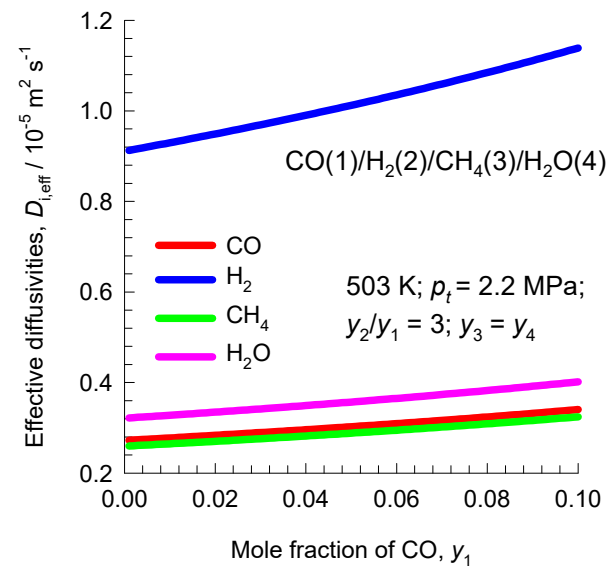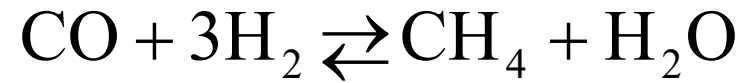
Surface reaction rate and flux for methanation reaction
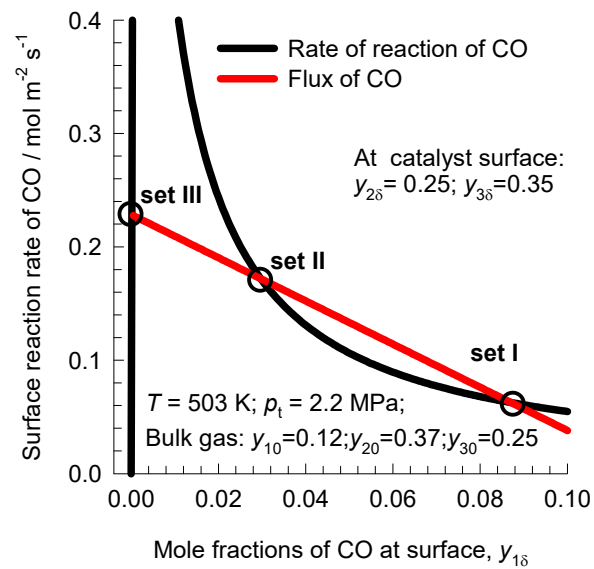
Composition profiles in "Film" Methanation reaction

$$CO + 3H_2 \rightleftarrows CH_4 + H_2O$$

Set I: $\sigma = 0.716$
Set II: $\sigma = 2.95$
Set III: $\sigma = 6.83$

H_2

CH_4

$CO(1)/H_2(2)/CH_4(3)/H_2O(4);$
503 K; $p_t = 2.2$ MPa

CO

Gas phase mole fractions in diffusion layer

Dimensionless distance, η

Bulk gas

H_2

CO

H_2O

CH_4

Ni/Al$_2$O$_3$ Catalyst

Tube Wall

Diffusion layer, δ

$\eta=0$

$\eta=1$
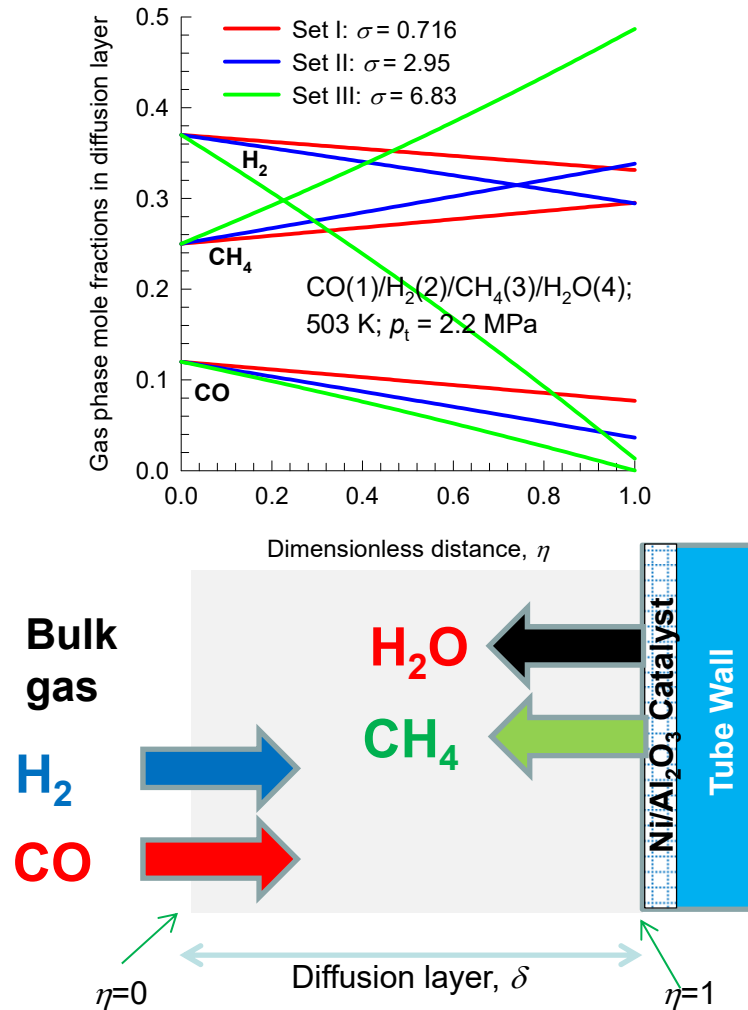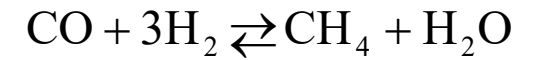
Composition profiles in "Film" Methanation reaction: equal M-S diffusivities

CO(1)/H$_2$(2)/CH$_4$(3)/H$_2$O(4); 503 K; p_t = 2.2 MPa

$$CO + 3H_2 \rightleftharpoons CH_4 + H_2O$$

Set I: σ = 1.27
Set II: σ = 9.2
Set III: σ = 13.3

Gas phase mole fractions in diffusion layer

H$_2$

CH$_4$

CO

$Đ = Đ_{13}$

Dimensionless distance, η

Bulk gas

H$_2$O

CH$_4$

H$_2$

CO

Ni/Al$_2$O$_3$ Catalyst

Tube Wall

Diffusion layer, δ

η=0

η=1

Effective diffusivities in CVD

$$\text{WF}_6 + 2\text{SiH}_4 \rightarrow \text{W}_{(s)} + 2\text{SiHF}_3 + 3\text{H}_2$$
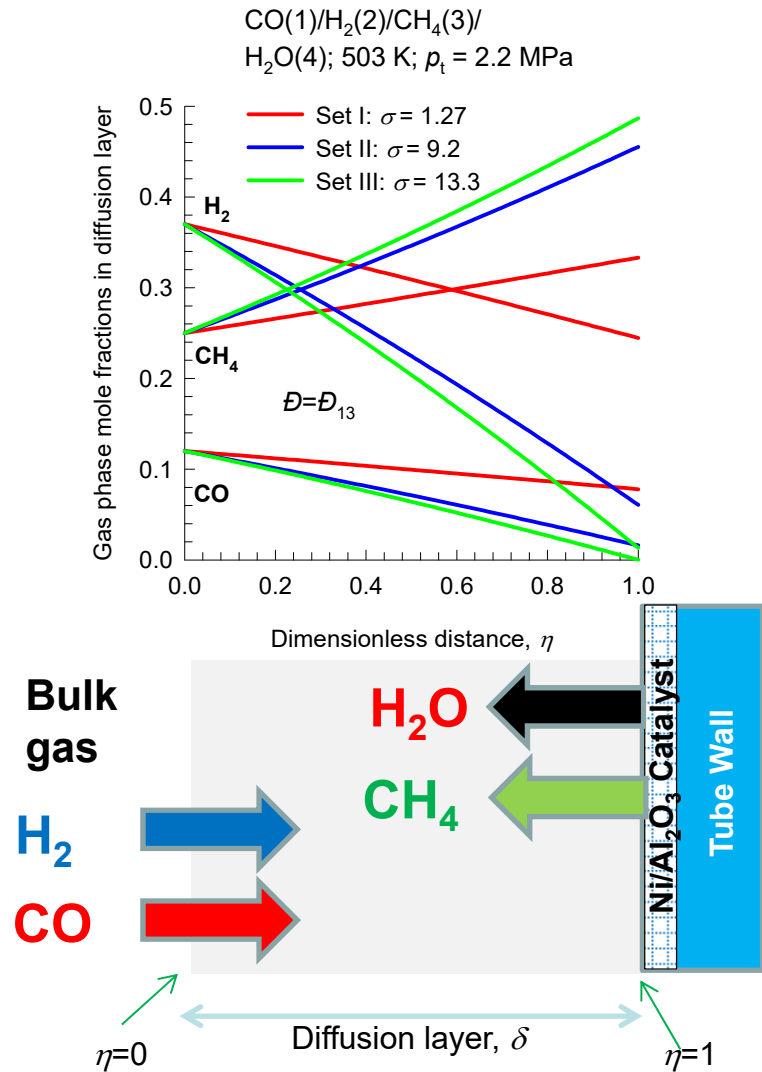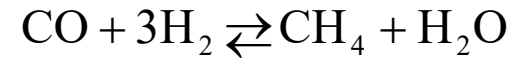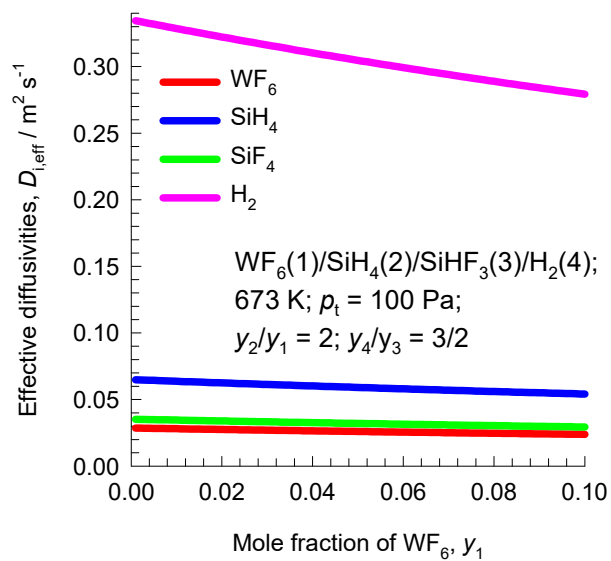
Fig. S12

Surface reaction rate and flux for W deposition
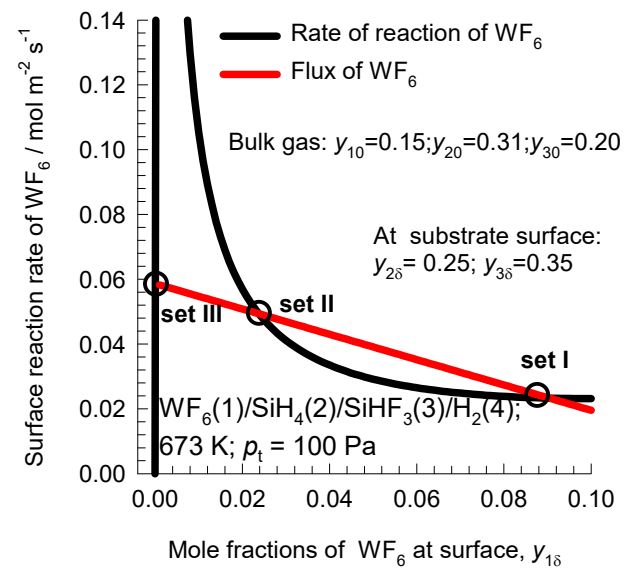
Composition profiles in "Film" CVD reaction

$$WF_6 + 2SiH_4 \rightarrow W_{(s)} + 2SiHF_3 + 3H_2$$
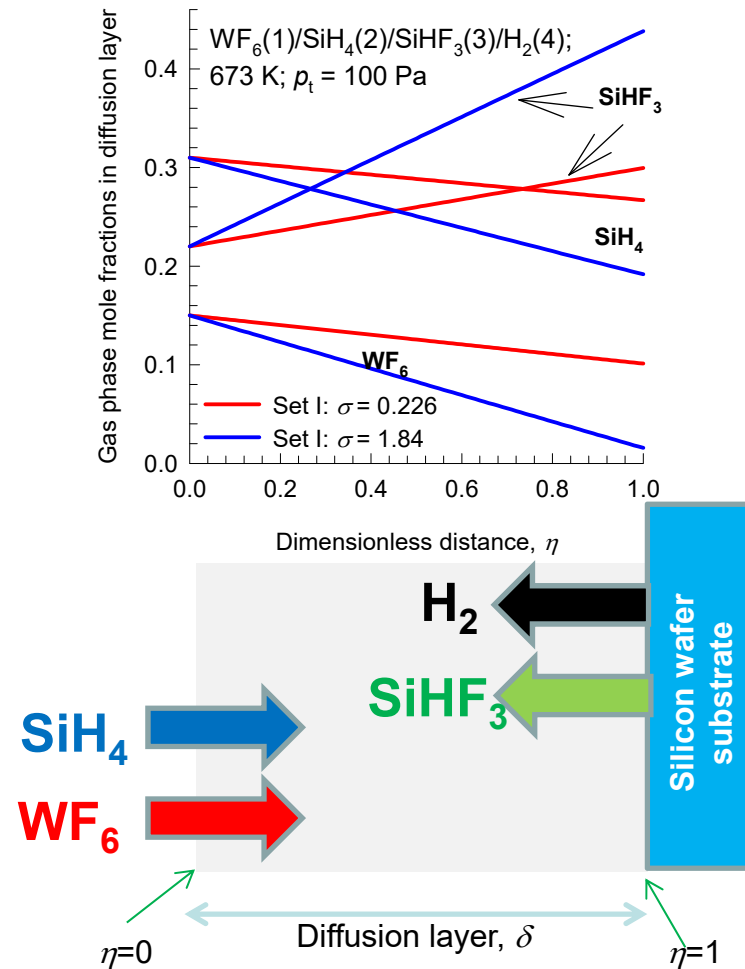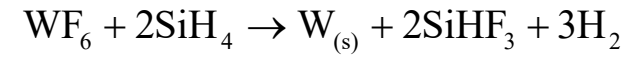
Composition profiles in "Film"
CVD reaction: all M-S diffusivities equal

$$\text{WF}_6 + 2\text{SiH}_4 \rightarrow \text{W}_{(s)} + 2\text{SiHF}_3 + 3\text{H}_2$$
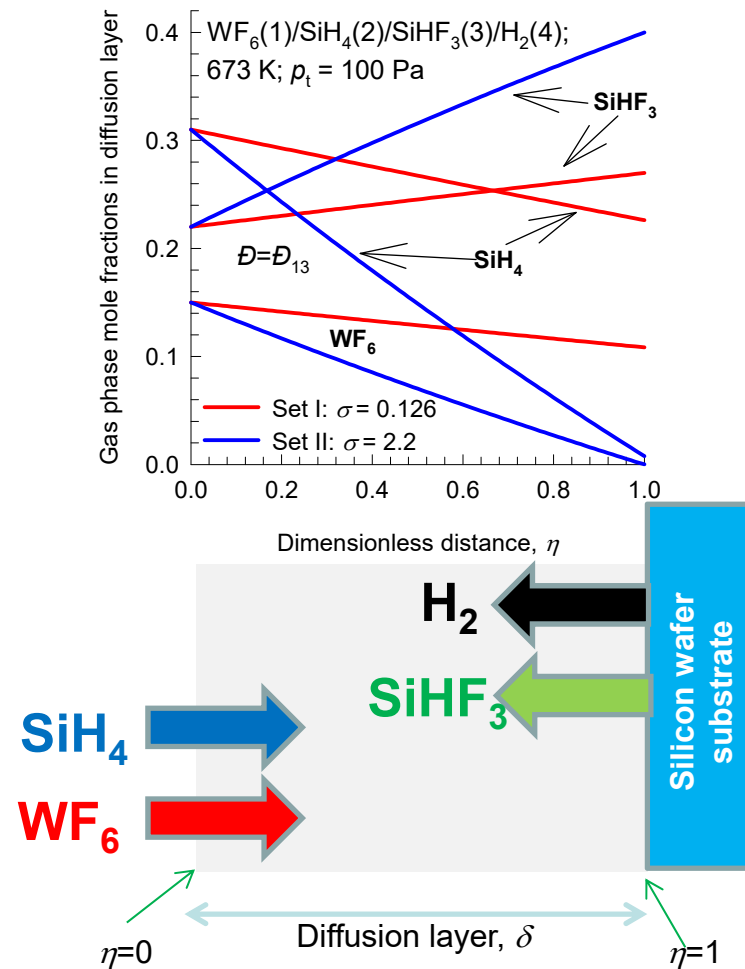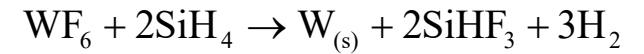
Fig. S15

Effective diffusivities in hydrogenation reaction

$$H_2 + C_2H_4 \rightleftarrows C_2H_6$$
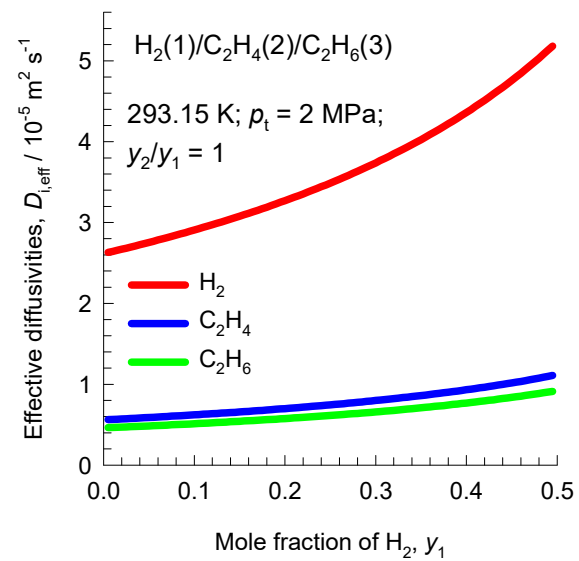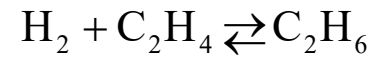
Surface reaction rate and flux for C_2H_4 hydrogenation reaction
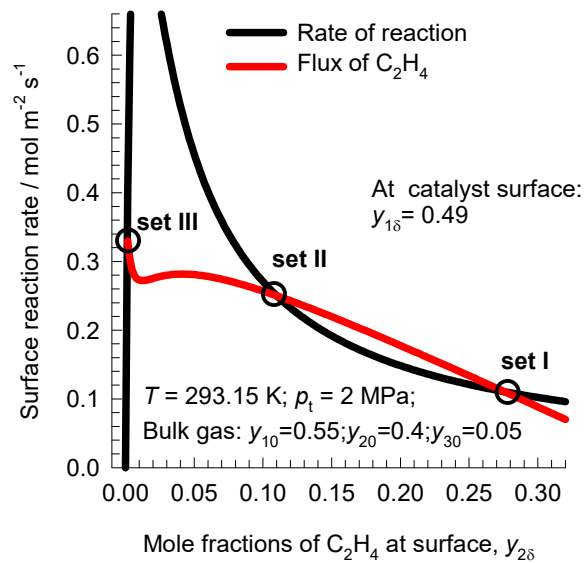
Composition profiles in "Film" Hydrogenation reaction

Fig. S17

$$H_2 + C_2H_4 \rightleftarrows C_2H_6$$
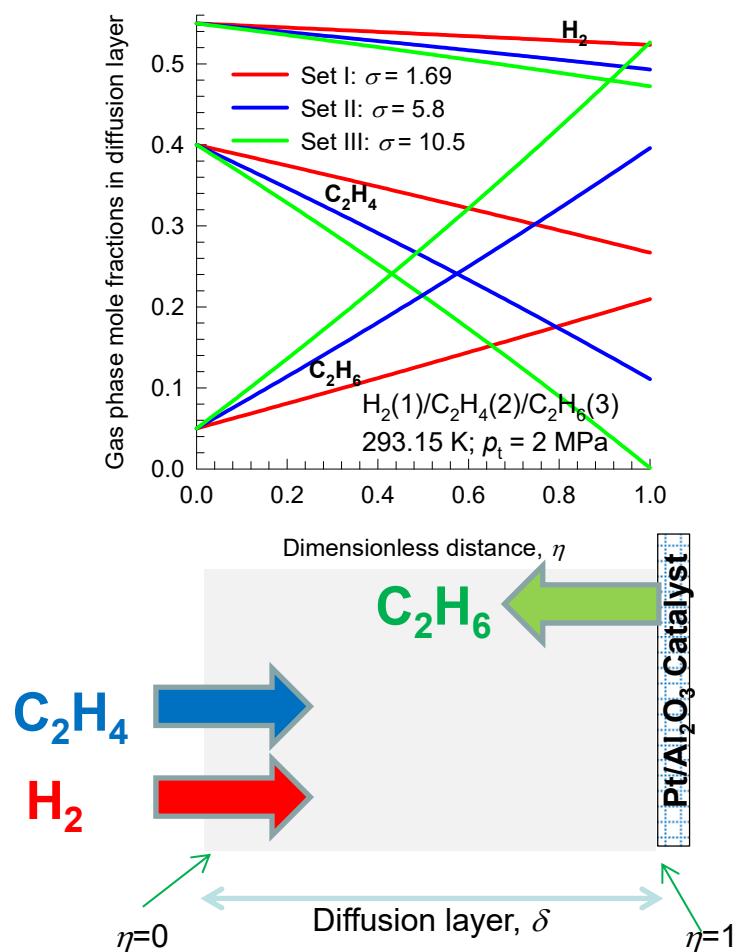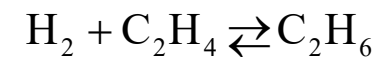
Effective diffusivities in oxidation reaction
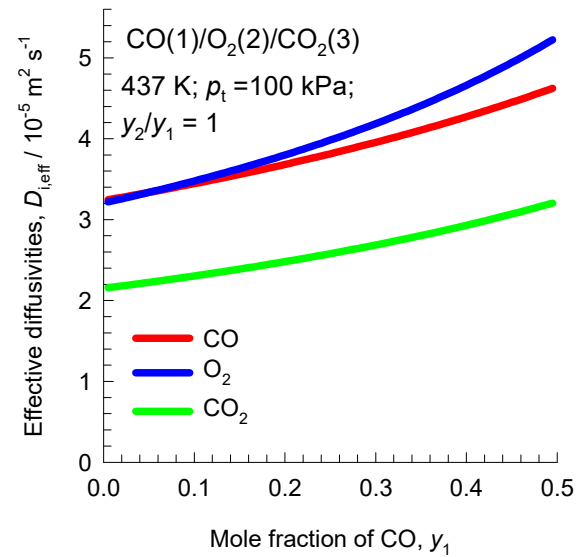
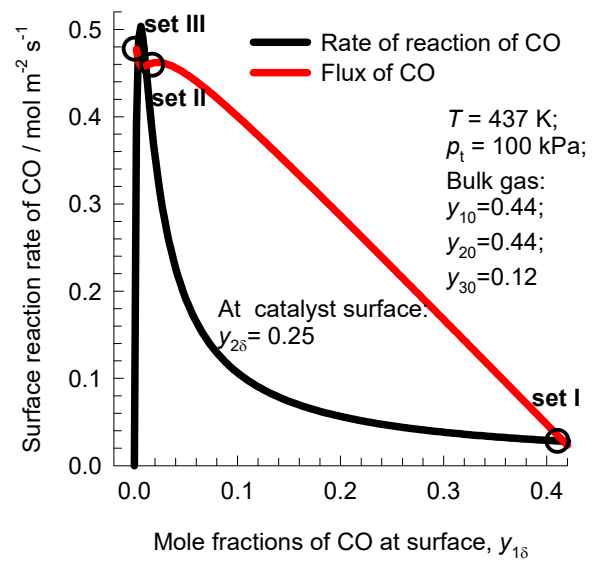# Surface reaction rate and flux for CO oxidation reaction

Composition profiles in "Film" oxidation reaction

Fig. S20